AN ASSESSMENT OF FRACTAL CHARACTERIZATION METHODS FOR $1/f^{\beta}$ PROCESSES WITH APPLICATION TO THE ANALYSIS OF STRIDE INTERVAL TIME SERIES

by

Alexander Schaefer

BS in Electrical Engineering, University of Pittsburgh, 2012

Submitted to the Graduate Faculty of

the Swanson School of Engineering in partial fulfillment

of the requirements for the degree of

Master of Science

University of Pittsburgh

2013

UNIVERSITY OF PITTSBURGH

SWANSON SCHOOL OF ENGINEERING

This thesis was presented

by

Alexander Schaefer

It was defended on

July 24 2013

and approved by

Ervin Sejdić, Ph.D., Assistant Professor, Department of Electrical and Computer Engineering

Amro El-Jaroudi, Ph.D., Associate Professor, Department of Electrical and Computer Engineering

Steven Levitan, Ph.D., John A. Jurenko Professor, Department of Electrical and Computer Engineering

Thesis Advisor: Ervin Sejdić, Ph.D., Assistant Professor, Department of Electrical and Computer Engineering

AN ASSESSMENT OF FRACTAL CHARACTERIZATION METHODS FOR $1/f^{\beta}$ PROCESSES WITH APPLICATION TO THE ANALYSIS OF STRIDE INTERVAL TIME SERIES

Alexander Schaefer, M.S.

University of Pittsburgh, 2013

The time evolution and complex interactions of many nonlinear systems, such as in the human body, result in fractal types of parameter outcomes that exhibit self similarity over long time scales by a power law in the frequency spectrum $S(f) = 1/f^{\beta}$. The scaling exponent β can be interpreted as the degree of fractal characteristic and thus as a "biomarker" of relative health and decline. This thesis presents a thorough numerical analysis of fractal characterization techniques with specific consideration given to experimentally measured gait stride interval time series. The ideal fractal signals generated in the numerical analysis are constrained under varying lengths and biases indicative of a range of physiologically conceivable fractal signals. This analysis is to complement previous investigations of fractal characteristics in healthy and pathological gait stride interval time series, with which this study compared. The comparative numerical analysis and experimental applications provide a thorough basis for determining an appropriate and robust method for measuring and comparing a physiologically meaningful biomarker, the spectral index β. In consideration of the constraints in applications, the significant drawbacks of proposed time domain methods are noted, and it is concluded that time-scale domain wavelet methods can provide a reasonably consistent and accurate biomarker technique for these fractal time series.

Keywords: fractals, time series analysis, self similarity, gait, stride intervals, DFA, wavelets, 1/f process

TABLE OF CONTENTS

1.0 INTRODUCTION 1

1.1 Overview of Human Gait 1

1.2 Functional Decline in Gait 4

1.3 Analysis of Gait Impairments 5

1.4 Research Objective 8

2.0 BACKGROUND 11

2.1 Fractal Time Series Analysis 11

2.1.1 Fractal Mathematics 11

2.1.2 Fractal Time Series 14

2.2 Algorithms for Estimation of Fractal Characteristic 22

2.2.1 Time Domain 22

2.2.1.1 Dispersional Analysis 22

2.2.1.2 Scaled Window Variance 22

2.2.1.3 Detrended Fluctuation Analysis 23

2.2.2 Frequency Domain 24

2.2.3 Time-Scale Domain 25

3.0 NUMERICAL ANALYSIS SCHEME 27

3.1 Evaluation of Algorithms 27

3.1.1 Discrete $1/f^{\beta}$ Process Generation 27

3.1.2 Numerical Analysis of Simulated Time Series 28

3.1.3 Numerical Analysis of Stride Interval Time Series 28
4.0 RESULTS 33
4.0.4 Overall Theoretical Performance 33
4.0.5 Effects of Nonzero Mean 41
4.0.5.1 Added Unit Mean 41
4.0.5.2 Removal of Mean 42
4.0.6 Gait Stride Interval Analysis 43
5.0 DISCUSSION 45
5.1 Simulated Signals 45
5.2 Stride Interval Time Series 47
6.0 CONCLUSIONS AND FUTURE WORK 49
6.1 Conclusions 49
6.2 Future work 50
7.0 ACKNOWLEDGEMENT 51
BIBLIOGRAPHY 52

LIST OF TABLES

3.1 Stride Interval Time Series, Study II 32
4.1 Comparative Analysis for Time Series, Study I 43
4.2 Comparative Analysis for Time Series, Study II 44

LIST OF FIGURES

1.1 Human Gait Cycle 2
1.2 Gait Analysis Techniques 6
2.1 von-Koch Curve Fractal 12
2.2 Scale Invariant Feature of von-Koch Curve Fractal 13
2.3 Exact and Statistical Fractals 14
2.4 Range of fGn and fBm Class Signals 19
2.5 Fractal Signals and Corresponding PSD Regression 20
3.1 Simulated Time Series - Cases 1 - 3 29
3.2 Stride Interval Time Series and PSD of Healthy Subject 30
3.3 Stride Interval Time Series and PSD of ALS Subject 32
4.1 Mean square error versus β, n = 100, 10,000 34
4.2 Mean square error versus n, β = 0, 1, 2 36
4.3 Mean square error versus β, n = 100, 600, 2,500, 10,000 38
4.4 Mean error versus β, n = 100, 600, 2,500, 10,000 39
4.5 Standard deviation versus β, n = 100, 600, 2,500, 10,000 40
4.6 Mean square error versus β, n = 100, 10,000 with unit mean 41
4.7 Mean square error versus β, n = 100, 10,000 zero mean 42

1.0 INTRODUCTION

1.1 OVERVIEW OF HUMAN GAIT

Human walking, or gait, is a complex process which is influenced by external stimuli and controlled and regulated by many phyiological systems and parameters. In a broad sense, human walking consists of repetitive and periodic movement of lower body segments. Though the entire walking process is controlled and modulated by many systems, the following is a simplified overview of the phases of one complete cycle of the physical process. The objective of this simplification is to define the gait process in terms of several functional phases for a consistent approach to analysis [1,2]. These individual phases separate the different motions and physical segments of one complete gait cycle, and thus allow the distinction of different control, feedback, and external mechanisms in the process. Here, the gait process begins with one foot's initial contact phase and ends with the same foot's subsequent contact phase [1–4]. An overview of each phase of the gait process (a) - (h) is given below and illustrated in Figure 1.1.

(a) Initial contact: This phase begins when the foot first makes contact with the floor. The position in which this happens influences the limb's loading response, and thus the pattern of the subsequent phase [1,2].

(b) Loading response: The loading response phase begins with the foot's initial contact and continues until the other foot is lifted for swing. Here, the lower ankle, knee, and leg flex for shock absorption to maintain maximum surface contact between the foot and the floor [1,2].

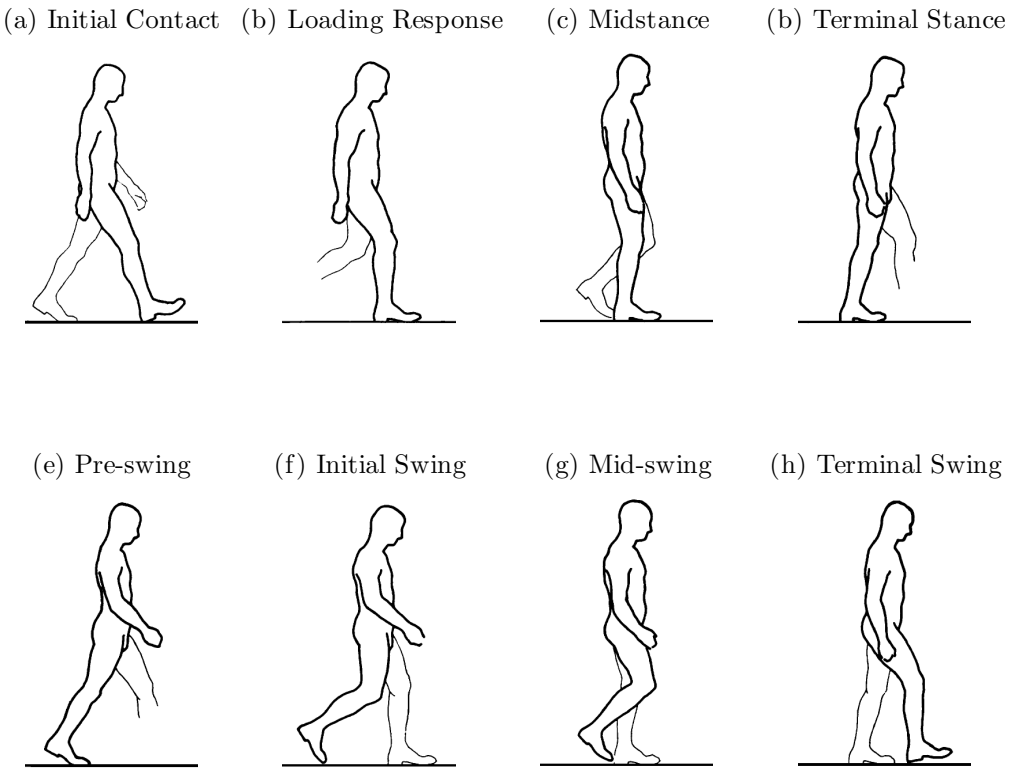

Figure 1.1: Human Gait Cycle, from [2]

(c) Midstance: The midstance phase is the beginning phase of the support interval where the other foot is in swing. Here, the foot's surface contact is maintained and the knee and hip extend [1, 2].

(d) Terminal stance: The terminal stance phase is the primary movement of this support interval. The knee remains extended, and the ankle rocks forward so that the foot's surface contact is still maintained. The body's weight and limbs move ahead of the forefoot [1, 2].

(e) Pre-swing: This is the last phase of the gait cycle in which the leg and foot are in constant stance. The foot's contact is shifted into the toe-off orientation in order to position the leg for swing [1, 2].

(f) Initial swing: The leg swing begins with the initial swing, the first of three phases of the entire swing period. The toe-off orientation from the previous pre-swing phase ends as the foot is completely lifted from the floor by flexing the knee and hip and carrying the body weight forward by the opposite limb's stance [1, 2].

(g) Mid-swing: This phase, in the middle of the swing period, exists when the limb is positioned opposite to the stance limb. The ankle's neutral position and the knee's flexion are maintained while the hip continues to carry the limb through to the end of the swing [1,2].

(h) Terminal swing: The terminal swing phase is the final of the swing period and concludes when the foot again strikes the floor. This consists of moving the limb ahead of the stance limb by hip flexion and knee extension. The ankle position remains neutral for the subsequent initial contact, thus completing the entire gait cycle [1, 2].

The separation of the entire gait process into these eight phases allows a more clear identification of each phase's specific functional objectives and the unique synergistic motions of all the physical components [1–4]. Past investigations into the gait process may have considered one or several specific events which may occur between or within each of the above defined phases [1]. This observation of the gait process not only lacks consistency, but may fail to recognize the influence of previous or subsequent phases. Previously, the beginning of the gait cycle was defined by an event referred to "heel strike" [2]. However, in the case of a person presenting abnormal gait, the heel may never contact the ground, or may do so at a later time in the overall process [1, 3, 4]. Also, there may be instances where heel and forefoot contact occur simultaneously [1,2]. This definition of gait as an eight phase process was introduced to resolve the potential ambiguities that pathological cases of gait may present to analysis of unique abnormalities.

1.2 FUNCTIONAL DECLINE IN GAIT

The human body is comprised of many physiological systems which interact in a nonlinear manner [5–12]. Accordingly, changes in functional outcomes in a given physiological system may be caused by trends in either one or many other systems [5,6,13]. Disease, aging, genetic disorders, and trauma can have significant effects on many physiological functional outcomes like gait [3, 4, 14–16]. Such a complex system is the locomotor system, which consists of a group of components from the central nervous, musculoskeletal, and other physiological systems. A general description of the locomotor system consists of the cerebellum, the motor cortex, and the basal ganglia, as well as visual, vestibular, and proprioceptive sensors [3, 4]. This may be seen as a generalized control system. The cerebellum and basal ganglia receive information for processing, and sends control signals by the motor cortex. Current state information and feedback are provided by internal and external inputs from proprioceptive and sensory nerve and visual signals [3, 4, 6]. In a healthy subject, a stable walking pattern is maintained by the constant dynamic interaction between all of the components of the locomotor system.

Neurophysiological changes may alter the locomotor system's ability to correctly modulate dynamic changes in the gait process [16]. For example, decreased nerve conduction velocity, loss of motor neurons, decreased proprioception, muscle strength, and central processing capabilities are notable declines due to advancing age [16]. Amyotrophic Lateral Sclerosis (ALS) is a neurodegenerative disease which severely affects the function of the motor neurons of the cerebral cortex, brain stem, and spinal cord [15]. Muscle weakness, increased fatigue and decreased endurance are characteristic of ALS [17] [18]. The direct consequence of these changes is an overall decreased in walking velocity, resulting in increased stride interval time. Parkinson's Disease (PD) and Huntington's Disease (HD) are both neurodegenerative diseases which affect the basal ganglia [16]. PD and HD are marked by irregular of central motor control, the most apparent outcome of which is a choreiform or "dancing" like gait [19] [16]. One common feature among all of these disorders is increased

stride interval time [16]. However, increased stride interval time alone is generally not indicative of any neurodegenerative disease, so the fluctuations of the stride interval must be considered to reveal any unique mechanisms of decline [15,16]. It is apparent that in general, such changes to components of the locomotor system from disease and aging result in abnormal gait. However, the identity and severity of the underlying mechanism(s) causing the functional decline are still unknown, and can be extremely difficult to identify and characterize due to the highly nonlinear and complex interactions of the constituent physiological systems [15, 16, 20, 21].

1.3 ANALYSIS OF GAIT IMPAIRMENTS

Analysis of the gait process is inherently challenging. Given the high number of time variant physiological systems and their according parameters, a complete quantitative perspective of the gait process has very high dimensionality [22]. For example, parameters of some general neural and physical processes may consist of the kinematic and kinetic data of joint angles, moments, and velocities, in addition to anthropometric parameters such as electromyographic, metabolic, and other data [1, 22]. Given the immense amount of critical variables in the process, some alternative methods which to reduce the amount of data but retain relevant information are necessary [1, 22].

Physiologists recognize the need for an effective and robust techniques to reduce and extract useful information from highly correlated time-dependent gait data [3, 4, 22–24]. Such techniques would greatly expand the understanding of motor control mechanisms and have immense benefit for monitoring disease progression and applying appropriate therapies [15, 22, 23]. Extensive investigations into various approaches to gait analysis are abundant in the literature, Figure 1.2 overviews some of these derived from a broad range of fields such as physics, engineering, computer science, psychology and cognitive science [5,8,9,22,23,25–27].

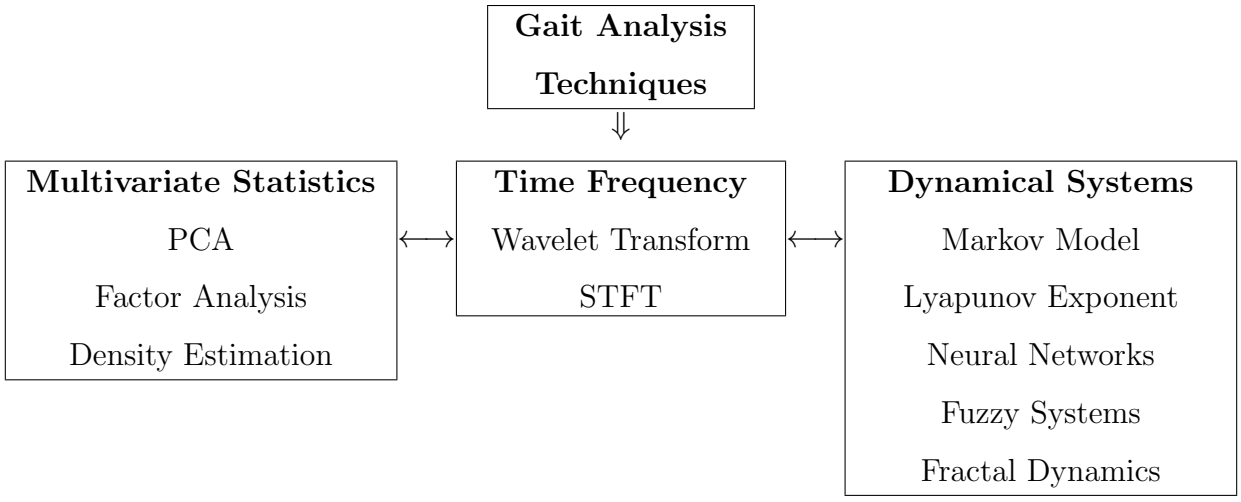

Figure 1.2: Gait Analysis Techniques

With such a wide variety of available analytical tools, the determination of an appropriate method to investigate health and decline in gait data is also difficult. In many cases, the choice of an analytical method is generally dictated by the nature of the available data. The main challenges of the gait analysis problem these methods aim to address are the high dimensionality and variability, temporal dependence, and nonlinear relationships of gait data [22]. To address the problem of high dimensionality and variability, multivariate statistical methods such as principal component analysis, factor analysis, and density estimation have been shown to provide insight into interpretations of gait data [22]. However, these statistical methods are significantly limited by the assumption of linearity between gait variables, and become intractable when considering more than five variables [22]. Due to differences in experimental design, instrumentation, and test subjects, statistical measurements of gait parameters fluctuate largely between similar trials [1, 22]. As a result, the high variability of statistical measures between various studies makes strictly statistical conclusions drawn from gait data more tenuous [22]. Finally, in physiology the time evolution of variables and systems in a considered process is critical. In gait processes, model parametrization of the time evolution of parameters assumes stationarity, and thus time sensitive patterns in the

gait process are not captured by these models [6,8,9,22,27]. Dynamical system models such as the Maximum Lyapunov Exponent have been developed to describe gait processes under random perturbations, but cannot inherently reveal the underlying mechanism governing the system behavior [6,24,28]. The nonlinear relationships between gait parameters is a natural observation of the inherent dynamics of the constituent systems, but such relationships evade traditional analytical description [6,22].

Clearly, alternative methods are necessary to address the inherent complexity and behavior of the variability of the gait data. Such alternative methods which may reliably quantify these characteristics are artificial neural networks, fuzzy analysis, and fractal analysis. Artifical neural networks have been shown to be a promising alternative tool, but implementations are complicated and lack an easily interpretable result [22]. Fuzzy and fractal analysis have also been indicated to show promise as physiological tools in a clinical setting [8, 9, 22, 27]. The significant distinction between these two is that fuzzy analysis treats variability as non-probabilistic uncertainty, whereas fractal analysis considers variability to be correlated and the outcome of long range dynamics [6, 8, 9, 22, 27]. Interestingly, the random fluctuations observed in the locomotor system present outcomes that are not random and uncorrelated, but appear to exhibit some correlation [3, 4, 14–16]. Recall that the interaction and dependence of each component of the locomotor system results in unique and complex functional changes in each phase of the gait process. Accordingly, these declines will have an effect on the time duration of one or more of the gait phases. To observe the overall fluctuation of altered dynamics due to each phase in the overall gait process, the stride interval is considered. This is defined as the time between subsequent initial contact phases, and its value is considered the output of the locomotor system [1–4, 14–16, 22]. Past analyses of stride intervals suggest that subsequent strides are influenced by recent strides, and have indeed shown that these correlations in stride exhibit not just short but very long range dependence (hundreds of steps) in a power-law fashion [3, 4]. Thus, the understanding of physiological processes as scale invariant parameter fluctuations provides a simple distinction between healthy and pathological processes [14–16]. In this case, the absence of scale invariance in

gait stride intervals may indicate presence or identity of pathology in one or more of the critical components of the locomotor system. By invoking the concept of fractal feature scaling, the investigation of the existence of these features can provide meaningful insight into the presence and severity of physiological decline. Thus, there is a need to find a computational tool which can reliably characterize the degree of scale invariance in the gait process.

1.4 RESEARCH OBJECTIVE

Fractal analysis techniques show promise as tool for developing computational biomarkers of decline due to disease, trauma, and aging. This work seeks to solidify the foundation of fractal analysis as a medical diagnostic tool, and to make clearer a direction to progress toward the long term goal of developing computational biomarkers. Reviews of the current techniques have indicated that promising alternative methods such as fractal analysis, fuzzy clustering, and artificial neural networks still require additional inquiry to clarify their potential as a phsyiological analysis tool, and here to the application of gait analysis. Fractal analysis shows significant promise for providing insight into gait processes that is not attainable with the aforementioned traditional methods. The clinical applicability and accessibility of fractal time series analysis here is an important goal. To these ends, this work mainly aims to quantify the performance of fractal time series analysis under ideal and constrained conditions, and to demonstrate the utility of these methods to signals derived in a physiological setting.

The first primary aim of this thesis is to clarify the interpretations of time series analyses for identifying the fractal properties of $1/f^{\beta}$ type scale invariant processes and highlight the inherent limitations of common methods. To validate the concept of fractal time series analysis, a number of established time, frequency, and time-scale domain estimation techniques will be implemented. Next, this investigation will observe the types of processes in which a variety of these techniques are most effective. The tests will include the entire range of $1/f^{\beta}$

processes, with special consideration given to simulated signals most indicative of physiological processes. A matter which is often obfuscated in other studies of fractal analysis is the choice of a metric for the fractal characteristic. For consistency, the process parameter β, also referred to as the spectral index, will be used as a metric for the fractal characteristic. The parameter β is convertible to other values commonly referred in the literature such as the fractal dimension D, the Hurst exponent H, and the scaling index α [6]. These relationships will be explored, however, β it is chosen for use here for its ease in interpretation with respect to the power law spectrum of $1/f^{\beta}$ processes, and thus its utility as a biomarker.

A second aim is to address the applications of these techniques to time series obtained in a physiological setting and their inherent constraints. A common limitation in acquiring physiological data, such as gait stride intervals, is the time series length [6, 26, 29]. In many instances, the physical limitations of the test subject, equipment design, and other factors of the experimental setting limit the available length of acquired data. It is therefore important to evaluate these techniques mindful of the constraints characteristic of the settings in which to apply them. Accordingly, this thesis will provide an evaluation of the algorithms with respect to short and long time series. It has also been recognized that the parameters of many physiological processes, such as stride interval time series, are by nature not zero mean [3, 4, 14–16]. To understand the effect of a time series with a nonzero mean, the calculation accuracy of each method is considered under three cases: (1) the normalized signal (2) the normalized signal with positive unit mean (3) a zero mean signal from the normalized signal minus its mean.

Finally, to verify the efficacy of the methods in the physiological setting, each method will be applied to published gait stride interval time series. The spectral index is calculated for gait time series from subjects with Parkinsons Disease, Huntington's Disease, Amyotrophic Lateral Sclerosis (ALS) and healthy controls [4, 15]. The calculated values will be a comparative basis with respect to other studies aiming to determine long range correlations and fractal behavior of gait stride interval time series [3, 23].

The thesis document is outlined as follows: Chapter 2 provides the background concepts of fractal time series analysis. Chapter 3 describes methods for implementing fractal analysis, the numerical simulation procedure, and the evaluation of physiologically measured signals. Chapter 4 presents the results of the numerical and physiological analyses. In Chapter 5 is a discussion and interpretation of the results and in Chapter 6 a summary of the findings, recommendations, and the possible direction of future work.

2.0 BACKGROUND

2.1 FRACTAL TIME SERIES ANALYSIS

2.1.1 Fractal Mathematics

Originally conceived in geometry, the mathematical concept of fractals was invoked to explore the existence of scale independent features [6, 30–32]. Generally, complex fractal geometries are created by applying a basic rule of transformation (generator) to a simple geometric object such as a line, triangle, or square (initiator) [6, 32]. For example, the von-Koch curve, a "snowflake" fractal, is easily recursively constructed by a line initiator, and the generator is applied by an equilateral triangle at the midpoint the line, shown in Figure 2.1 The infinite iteration of transformations results in a geometry with the identically complex structure at all scale lengths. In Euclidean geometry, the set of numbers $\mathbb{R}^n$ for $n = 1, 2, 3$ are used to describe the shape and spacial coordinates of objects in space [6, 30]. However, the Euclidean description of inherently complex structures would essentially require a large number of objects and corresponding spacial coordinates to describe the geometry at all scales [6]. This property is exemplified by observing a shorter scale length of the von-Koch curve, given in Figure 2.2. Consequently, Euclidean coordinates in $\mathbb{R}^n$ for $n = 1, 2$ are insufficient to describe the von-Koch curve fractal on all different scales [6, 30–32].

A direct result of this recursively defined structure is that spaces of integer dimension are inadequate for completely representing it. Additionally, a set of traditional geometric axioms inherently cannot describe the outcome of the structure in the same way the re-

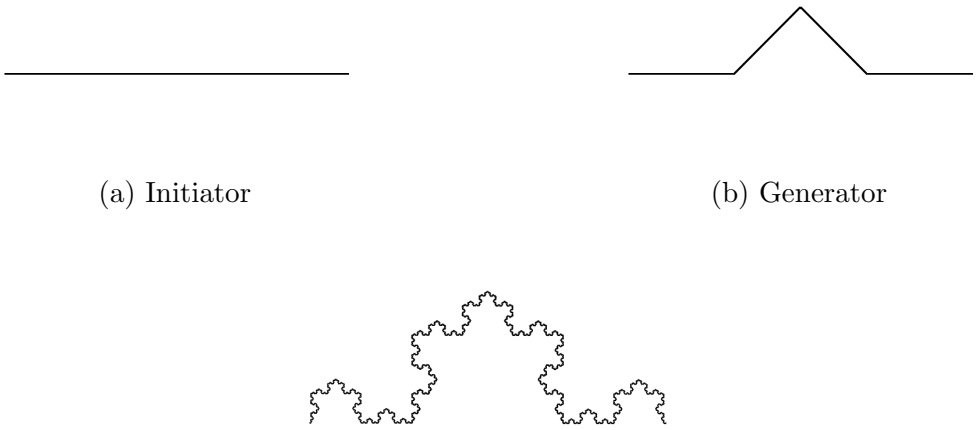

(a) Initiator

(b) Generator

(c) Fractal

Figure 2.1: von-Koch Curve Fractal

cursive algorithm can, which contains underlying mechanism of the outcome [6, 31, 32]. To accommodate the infinite scales of existence of the geometric features, spaces of non-integer dimension $\mathbb{R}^{n+d}$ where $0 < d < 1$ must be used [6, 30–32]. Since d is a fractional number, these spacial dimensions are "fractional", or henceforth referred as fractal. In this space, geometric axioms are relaxed and the algorithmic rules of order offer a shorter description of complex structures [6, 30]. In the instance of the von-Koch curve, the complex structure is given simply in terms of an initiator and generator. The general utility of fractal space then is a unique description of complexity by a simple recursive algorithm that captures the essence of the object. This is utilized in favor of whole integer space and Euclidean geometry requiring a large number of coordinates and axioms to attempt to describe an inherently complex object or process [6].

Mathematical, or exact, fractals generated by a recursive algorithm exhibit the same feature over an infinite range, providing the critical property of scale invariant self similarity. Naturally observed, or statistical, fractals exhibit feature scaling over a limited range. The Mandelbrot Tree, an exact fractal, and an arterial network, are shown in Figure 2.3 [6].

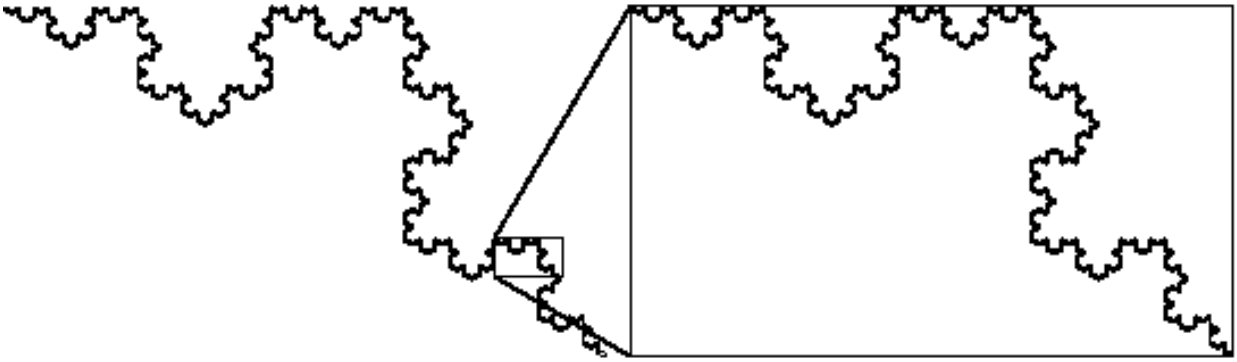

Figure 2.2: Scale Invariant Feature of von-Koch Curve Fractal

The infinite recursive iteration in the Mandelbrot Tree creates an identical branching feature which continues infinitely at all smaller and larger scale lengths. Comparatively, the branching feature in the arterial network is not exact, and the length scales on which these features exist is limited. However, the existence of this feature on many scales is a striking property. This suggests that the creation of this complex structure is the outcome of a simple recursive rule, and fractal analysis may provide valuable insight into the identity and behavior of this mechanism.

In a fractal object, a measurement of a parameter (feature) does not converge to any value on a single scale. Instead, a given parameter q exhibits a power law scaling relationship with respect to the scale s according to [6]

$$q = ps^{\varepsilon} \tag{2.1}$$

Here, p is the factor of proportionality and ε is the scaling exponent, and for inverse power law relationships is a negative number. The value of the scaling exponent can be easily found by the slope of a linear regression to the by rearranging Equation 2.1 into the relationship

$$\log q = \log p + \varepsilon \log s \tag{2.2}$$

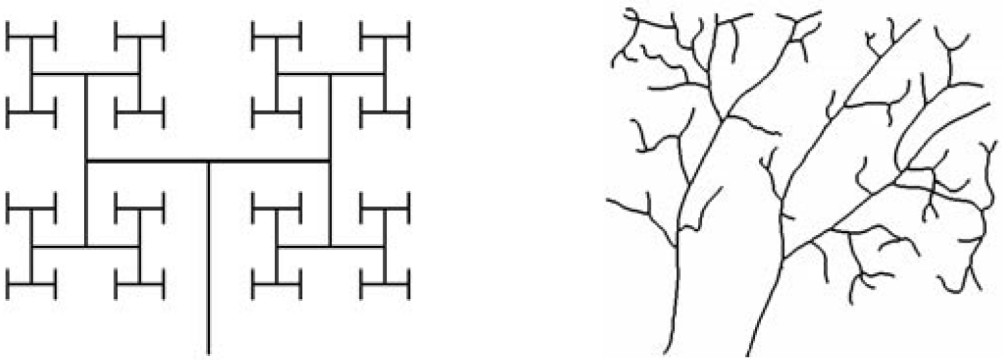

(a) Mandelbrot Tree

(b) Arterial Network

Figure 2.3: Exact and Statistical Fractals, from [6]

It is critical to be aware that the range of scales s is restricted for natural physical structures and phenomena. In general, the inverse power law scaling property of a parameter gives rise to the fundamental self-similarty and scale invariance inherent in a fractal object.

2.1.2 Fractal Time Series

The time series of many physiological processes' parameters such as arterial blood pressure, breathing, heart rate, and walking have been observed to possess complex statistical properties [8,9,12,16,21,25,33–35]. This phenomenon is due to the time evolution and complex interactions of many dynamical systems, imposed with random fluctuations, resulting

in chaotic processes [36]. Some descriptions of the statistical qualities of these processes may be of a slow exponentially decayed autocorrelation function, a $1/f$ type power spectral density, or a heavy-tailed probability distribution function [30, 37–39]. In such processes, consider the time evolution of variables represented by a time series $x(t)$. The process has the property of being long range dependent (LRD) when the autocorrelation function $r_{xx}(\tau)$ of $x(t)$ satisfies the following condition.

$$\int_0^\infty r_{xx}(\tau)\, d\tau = \infty \tag{2.3}$$

That is, the autocorrelation function is nonintegrable [30,40]. Accordingly, the nonintegrable autocorrelation function can be expressed in the following form

$$r_{xx}(\tau) \approx c|\tau|^{-\beta} \quad (\tau \to \infty) \tag{2.4}$$

where $c > 0$ and $0 < \beta < 1$. This relationship implies a power law and long range dependence in the autocorrelation of $x(t)$ [30]. Similarly, the autocorrelation function reveals special properties of the power spectral density $S(\omega)$ of $x(t)$

$$S(\omega) = \int_0^\infty r_{xx}(t) e^{-j\omega t}\, dt \tag{2.5}$$

In the case of a long range dependent time series, $S(\omega)$ does not exist in the above form [30]. However, when the autocorrelation function approximated by the power law $c|\tau|^{-\beta}$, the power spectral density can be found by

$$F(|\tau|^{-\beta}) = 2 \sin\left(\frac{\pi\beta}{2}\right) \Gamma(1-\beta)|\omega|^{1-\beta} \tag{2.6}$$

where F is the Fourier transform and Γ is the Gamma function [30, 41, 42]. It follows that the power spectral density of the long range dependent process also possesses the power law property, commonly denoted $S(f) = 1/f^\beta$ [30, 32, 35, 43].

The same principle for LRD time series $x(t)$ applies to the expression of the autocorrelation in terms of probability distribution function $p(x)$ given by

$$r_{xx}(\tau) = \int_{-\infty}^{\infty} x(t)x(t+\tau)p(x)\,dx \tag{2.7}$$

In the following expressions for the mean μ_x and variance σ_x^2,

$$\mu_x = \int_{-\infty}^{\infty} xp(x)\,dx \tag{2.8}$$

$$\sigma_x^2 = \int_{-\infty}^{\infty} (x-\mu_x)^2 p(x)\,dx \tag{2.9}$$

the integrals do not exist in the case of a long range dependent time series $x(t)$, indicating a heavy tailed probability distribution function [30, 44, 45]. In contrast to conventional time series in $\mathbb{R}^1$ space, a time series that is long range dependent and accordingly possesses the power law type ACS, $1/f$ PSD, and heavy tailed PDF is fractal and exists in $\mathbb{R}^{1+d}$ space where $0 < d < 1$ [30]. The existence of these properties are indicative of other unique characteristics which can reveal fractal behavioral mechanisms of the process beneath the apparent chaos [27, 30, 46]. Due to the long range dependence of such a time series, and the nonexistence of the mean and variance, such measures are insufficient to describe the statistical nature of such properties. The Hurst exponent H is useful for this purpose, and relates to the power law in the LRD autocorrelation [30]

$$r_{xx}(\tau) \approx c|\tau|^{2H-1} \quad (\tau \to \infty) \tag{2.10}$$

The goal of fractal time series analysis is an extension of fractal geometric analysis to establish a metric which can indicate the scale invariant nature of statistical and other properties of time evolving system parameters [23, 25, 26, 31, 32]. Strictly speaking, fractal time series cannot be self similar in the same sense geometries can be. Since the dimensions of a time series (amplitude versus time) are different, any apparent power law scaling of properties exhibits the property of self-affinity [6]. Mathematical and statistical fractal

geometries and structures are self-similar, whereas amplitude versus time processes are self-affine [6]. However, the distinction between self-similar and self-affine is not critical here, and altogether the description of power law behavior of parameters is referred to as self-similarity. Further, this thesis considers a multitude of fractal methods of self-affinity in the time, frequency, and time-scale domains. Each of these methods aims to reveal the critical property of the scaling of a feature q over the range s given by $q = ps^{\varepsilon}$. All methods fit a regression to the data $\log(q)$ versus $\log(s)$ for finding the scaling index ε as the linear regression slope [6]. The result is a useful observation and more concise description of the highly complex and apparently random fluctuations in a given time series. A critical assumption is that the resulting system description, in this case the scaling index, is time-invariant. Accordingly, this investigation considers monofractal time series analysis only, in which the fractal measure is assumed to not change with time. This is a simplification of multifractal fractal time series, in which the metric itself may exhibit time evolution [6,47,48].

It has been noted that the power spectral density is an informative perspective of fractal processes, which exhibits inverse power law scaling behavior by $S(f) = 1/f^{\beta}$. Processes of this type are henceforth referred to as $1/f^{\beta}$ processes [6, 23, 35, 43, 49, 50]. Generally $1/f^{\beta}$ process can be classified as belonging to one of two classes, fractional Gaussian noise (fGn) or fractional Brownian motion (fBm) [6, 26]. For fGn class signals, the probability distribution of a segment of the signal is independent of the segment size and its temporal position in the signal [6]. Thus, the correlation structure and any statistical descriptions of the process do not change over time, so the process is stationary [23]. In an fBm signal, the probability distribution in a larger segment is equal to a distribution in a smaller segment when the distribution in the large segment is rescaled [6]. Here, the inverse power law relationship is observed for the calculation of some statistical measure m on the segment of length n

$$\log m_n = \log p + H \log n \tag{2.11}$$

This is the same power law relationship given in 2.2, where p is a proportionality factor and H is the Hurst exponent and $H \exists [0, 1]$. The Hurst exponent is a commonly used metric for

indicating the fractal nature of a fractional Gaussian noise or fractional Brownian motion process [51], [52], [53]. These processes have the property that the cumulative summation of an fGn signal results in a fBm signal [6]. In general, a given process is interconvertible from one class to the other by the integral or derivative [6, 35, 43, 49, 50]. This necessitates a unique Hurst exponent specific to each class of processes. These can be denoted $H_{fGn} \exists [0, 1]$ and $H_{fBm} \exists [0, 1]$ [6, 26]. $H = 0.5$ in each class is the special case, where $H_{fGn} = 0.5$ is white Gaussian noise ($\beta = 0$) and $H_{fBm} = 0.5$ is Brownian motion ($\beta = 2$) [6, 23]. White Gaussian noise is the characteristic process of the fractional Gaussian noise class of $1/f^{\beta}$ processes [6]. The important property of white Gaussian noise is that energy is equally distributed for all frequencies. Thus, it has a flat power spectrum and $\beta = 0$. $H_{fGn} < 0.5$ is anti-correlated Gaussian noise, and $H_{fGn} > 0.5$ is correlated noise [23]. Brownian motion is the characteristic process for the fBm class. These processes exhibit a $1/f^{\beta}$ power spectrum where $\beta = 2$ [6, 15]. In this case, successive outcomes in the process are correlated, and the process exhibits non-stationary time evolution [23]. $H_{fBm} < 0.5$ is anti-persistent Brownian motion, and $H_{fBm} > 0.5$ is persistent Brownian motion, where $H_{fBm} = 0$ is pink noise of $1/f^{1}$ [6]. Shown in Figure 2.4 are fGn signals of $H = 0$, 0.5, 1 and their the corresponding (cumulatively summed) fBm signals, providing an overview of the signals of each process class and their interconvertible relationship.

In the case where $\beta = 1$, some correlation between timescales exists but is weak [26]. In summary, a given process can be classified as belonging to one of these two distinct classes where $\beta = 1$ is the distinct boundary between each [43]. The relationship between each class's Hurst exponent and the power spectrum $1/f^{\beta}$ can be observed by the by the following relationships [6]

$$H_{fGn} = \frac{\beta + 1}{2} \tag{2.12}$$

$$H_{fBm} = \frac{\beta - 1}{2} \tag{2.13}$$

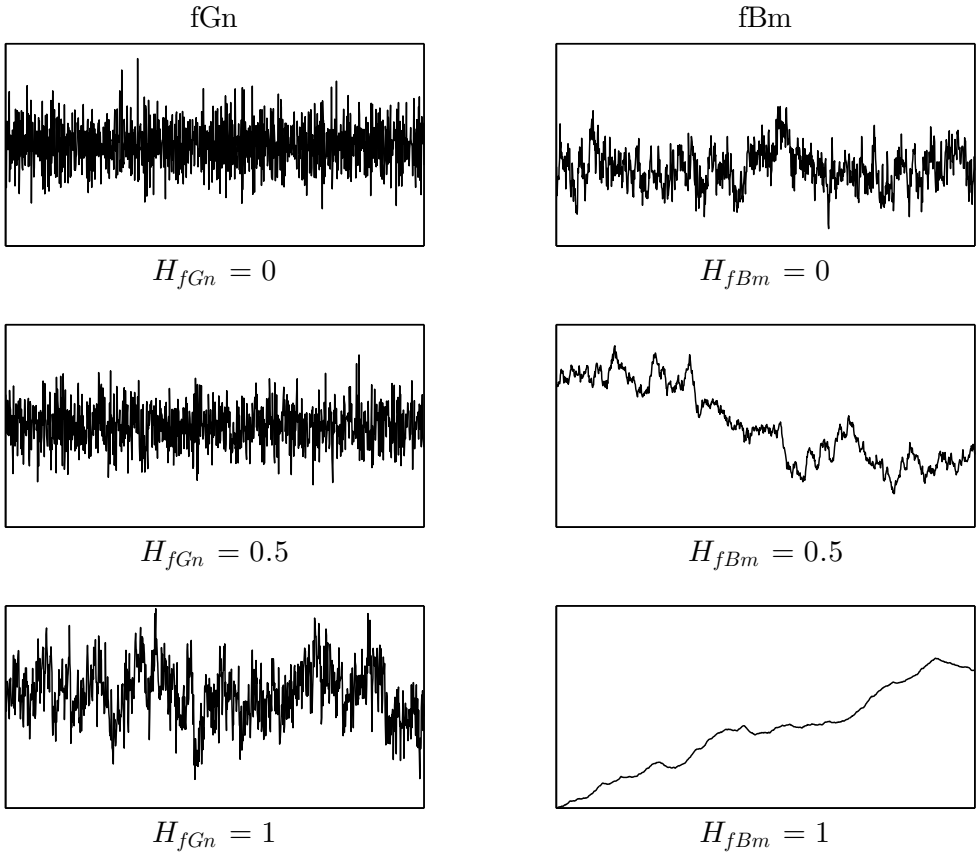

Figure 2.4: Range of fGn and fBm Class Signals

Thus, the range of all fGn and fBm processes for $0 < H < 1$ correspond to $-1 < \beta < 3$, where the boundary between each class lies at $\beta = 1$ [6, 26]. Figure 2.5 gives an overview of an fGn Gaussian white noise ($\beta = 0$), pink noise ($\beta = 1$), and fBm Brownian motion or red noise ($\beta = 2$). Adjacent to each signal is its its log-log power spectrum, and the linear regression with slope indicating the corresponding β value.

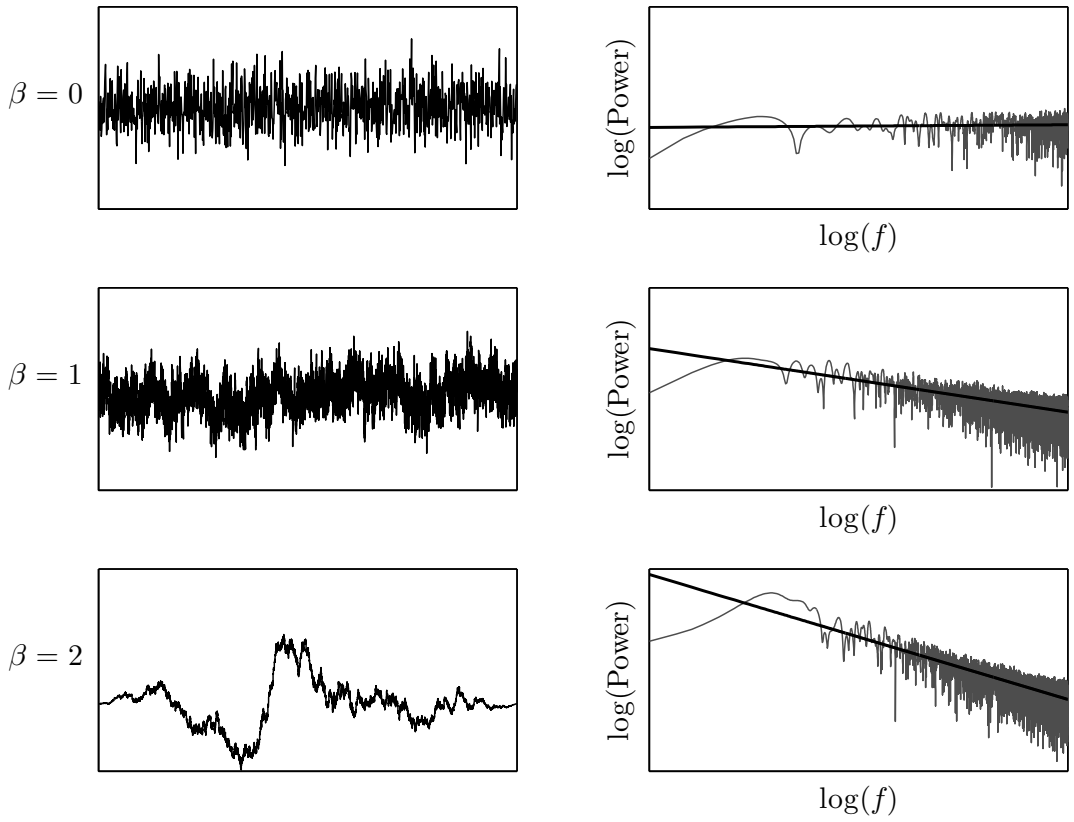

Figure 2.5: Signals of length N for β = 0,1,2, corresponding PSD and regression

Past investigations have indicated that for some complex time series, traditional signal processing techniques and models may fail to reveal new meaningful information about the process's unique patterns, self similarity, and statistical properties at many time scales [23, 26]. Parametric methods have been investigated to attempt to quantify and model complex

behavior in physiology such as [3, 6, 24]. However, these methods assume stationarity, time invariance, and linear dependence, and cannot recreate and characterize long range scaling of the parameter [3, 24]. This thesis is concerned only with the evaluation of the processes and algorithms which seek characterize H in the power law relationship $m_n = pn^H$. Insofar as the presence of a linear relationship in the equation $\log m_n = \log p + H \log n$ indicates the similarity of the statistical measure m_n on scale n, such signals are referred to as "self-similar" or "long-memory" processes which possess "long-range correlation" and "long-tailed statistics" [6, 10, 53]. In this paper, the nomenclature is simplified, and the observation of the inverse power law of a parameter at many time scales is simply said to be indicative of a fractal process. Again, this simplification is mindful of the goal to establish a metric and computational biomarker of health and decline. Thus, the focus of this investigation is solely on fractal time series analysis techniques and their utility in evaluating processes which are the outcome of complex physiological system interaction.

Many well developed fractal estimation algorithms for finding the Hurst exponent are specific to each process class. The choice of a method to evaluate the fractal properties of a signal will accordingly be difficult in a setting where it is unclear which of the two classes the signal belongs. If such methods are inappropriately applied, the calculated class specific Hurst exponent will be incorrect. Consequently, its interpretation as a physiological biomarker will be ambiguous and potentially misleading. Awareness of this hazard is especially critical whenever the process lies at the boundary between fractional Gaussian noise and fractional Brownian motion. This case, when $\beta = 1$, a signal represents the type of fractal process most typically exhibited by physiological systems [6, 7, 9–12, 34]. The application of so called class specific algorithms in this case is not recommended. As a result of this dichotomy, signal classification, the choice of a fractal characterization method, and the interpretation of its result becomes a critical yet inherently difficult procedure which this thesis seeks to clarify.

2.2 ALGORITHMS FOR ESTIMATION OF FRACTAL CHARACTERISTIC

For a $1/f^{\beta}$ process, β values can be estimated in time, frequency or time-frequency (time-scale) domains. Here, we overview several most prominent implementations in literature concerned with characterizing physiological phenomena.

2.2.1 Time Domain

This section overviews the three time domain fractal techniques implemented here. These are dispersional analysis, bridge detrended scaled window variance (bdSWV), and detrended fluctuation analysis (DFA).

2.2.1.1 Dispersional Analysis For dispersional analysis, we refer to the proposal of this technique by Bassingthwaighte, et al [20, 21, 54, 55]. This time domain based algorithm is a one dimensional approach that estimates the variance of the signal at many different time scales. For a given signal of length N $[x(i)]_{i=1}^{N}$, first the mean is calculated in adjacent non overlapping intervals of size 2^m, and the standard deviation of the means is found. This evaluation continues for $m = 1, 2, ..$ on the condition that the number of intervals $n = N/m \geq 4$, where calculation of the standard deviation would overly bias the estimate [6, 54]. Then, the standard deviation of each interval is plotted versus the interval size on a log-log plot. A standard linear regression to this plot will have a slope indicating the fractional Gaussian noise Hurst exponent H_{fGn}, and thus the spectral index is found by $\beta = 2H_{fGn} - 1$ [6]. Theoretically indicated to work only for fGn processes, the results for calculation of fBm class signals ($\beta > 1$) are not tenable [6].

2.2.1.2 Scaled Window Variance For evaluating processes by scaled window variance, we refer the method proposed by Cannon, et al [6, 26, 51, 56]. This is part of a class of time domain fractal methods similar to dispersional analysis based on calculating variance on increasing sized intervals of the signal. This method introduced a modification to dipersional

analysis where a local trends on each interval is removed. In this method, bridge detrending is implemented to remove the local trend, and the technique is referred to as bridge detrended scaled window variance (bdSWV). The signal is divided into non overlapping intervals of size from $n = 2^i, .., N$ for $i = 0, 1, ..., N$. The data in each interval is detrended by subtracting the "bridge", a line connecting the first and last points in the interval. Then, the standard deviation is calculated for each detrended interval. Finally, the standard deviation of each interval is plotted versus the interval size on a log-log plot. A standard linear regression to this plot will have a slope indicating the fractional Brownian motion Hurst exponent H_{fBm}, and the spectral index is found by $\beta = 2H_{fBm} + 1$ [6]. Contrary to dispersional analysis, the modifications introduced in this method were aimed to accurately calculate fractal properties of fBm processes, and the results of fGn calculations are not theoretically tenable.

2.2.1.3 Detrended Fluctuation Analysis The approach for calculating the fractal index by detrended fluctuation analysis (DFA) is provided by Peng, et al [13, 34, 57], and it has been thoroughly evaluated by others for many applications [29, 33, 58–65]. DFA is a time domain based algorithm, and calculates the proposed "scaling exponent" α which is a useful to indicate the randomness of a time series over the boundary between fGn and fBm processes. The spectral index β is related to the DFA parameter α by [6]

$$\beta = 2\alpha - 1 \tag{2.14}$$

For the time series $[x(i)]_{i=1}^{N}$, the integration of the difference of series deviations its mean $\bar{x}$ is given by

$$y_i = \sum_{j=1}^{i} [x(j) - \bar{x}] \tag{2.15}$$

for $i = 1, .., N$. This series is then divided into $\lceil \frac{N}{n} \rceil$ non overlapping intervals of length n, where $\lceil x \rceil$ is the greatest integer operation. A least squares regression line is fitted to

the signal on each interval. The trend series is formed by the sequences of the regressions $[y_n(i)]_{i=1}^{N_n}$. The average fluctuation of the trend series is calculated by

$$F(n) = \sqrt{\frac{1}{N_n} \sum_{i=1}^{N_n} [y(i) - y_n(i)]^2} \tag{2.16}$$

Next, the interval length n is changed and the detrending and average fluctuation is calculated again. Considering the range of interval sizes is critical for accurate application of DFA [6, 16, 29]. The small and large interval lengths, n_l and n_m respectively, must be restricted in order to avoid calculating potentially large or small interval fluctuations that will bias the result. Additionally, the difference between subsequent intervals should be linear to properly recognize the relationship of $\log F(n)$ to $\log n$ [26]. Thus, we implement a general scheme where the smallest interval is restricted to $n_L = \lceil \frac{N}{100}, 10 \rceil$ and the largest interval to $n_M = \lceil \frac{N}{10}, 20 \rceil$. The interval size is increased $n + 10$ for each subsequent calculation to acquire a range of average trend series fluctuations $F(n_l), ..., F(n_M)$. Then, $\log F(n_i)$ vs $\log n_i$ is plotted for $i = 1, ..., m$. A standard linear regression to this plot will have a slope indicating the DFA scaling exponent α [6].

2.2.2 Frequency Domain

These techniques directly evaluate the power law scaling property of a fractal series' power spectral density. There are many available methods for performing the spectral estimation required to evaluate a fractal process's frequency domain $1/f^\beta$ power law [50, 61, 66]. Here, the periodogram method and Eke's ${}^{low}PSD_{we}$ method are implemented [5, 6, 26]. The periodogram method is used in calculating $S(f)$, the square of the FFT after applying a Gaussian window. The relationship

$$S(f) \propto 1/f^\beta \tag{2.17}$$

provides a direct basis for evaluating β with respect to the log-log linear regression of the power spectral density [6]. Eke improved on this method to more accurately characterize β

for both signal classes. First, for the time series $[x(i)]_{i=1}^{N}$ the mean $\bar{x}$ is subtracted. Next, a parabolic window is calculated and applied by

$$W(j) = 1 - \left[\frac{2j}{N+1} - 1\right]^2 \tag{2.18}$$

for $j = 1, .., N$. Finally, the bridge line connecting the first and last point of the signal is subtracted from the series. After calculating the power spectral density by the periodogram, all frequency estimates for $f < 1/8 f_{max}$ are omitted. Again, β is found by linear regression of the log-log power spectral density [6].

2.2.3 Time-Scale Domain

Time-scale techniques are investigated here for their value in providing scale variant behavior of the signal, of critical interest for a fractal process [6, 67–71]. The approach used here is based on the wavelet transform. This is especially informative, as it provides information of shifted and stretched, or rescaled, versions of the basis mother wavelet function [67]. Additionally, the wavelet transform is not biased for low and high frequency components of the process, and provides equally precise characterization of these dynamics [6]. The Average Wavelet Coefficient (AWC) method described by Simonsen and Hansen [69] is conveniently implemented for this function. For the continuous wavelet transform of signal $h(x)$, the mother wavelet function is given by

$$\psi_{a;b}(x) = \psi\left(\frac{x-b}{a}\right) \tag{2.19}$$

where in this case a twelfth order Daubechies wavelet is used [69]. The number of levels for the Mallat algorithm discrete wavelet transform is chosen with respect to the signal length, determined here as never lower than 2^3 or greater than 2^7 [72]. The mother wavelet is a zero-mean function, where a is the scale coefficient and b is the translation coefficient. This is used as a basis function for an integral transform given by [69]

$$W[h](a,b) = \frac{1}{\sqrt{a}} \int_{-\infty}^{\infty} \psi^*_{a;b}(x) h(x) dx \tag{2.20}$$

The result of the transformation provides the scale and transpose coefficients for the signal at the each of the prescribed levels. The wavelet transform is interpreted as a representation of frequency and time dilated versions of the mother wavelet function $\psi_{a;b}(x)$. To find the averaged wavelet coefficient $\bar{c}_n$ at level n, the arithmetic mean with respect to the translation coefficient b is calculated by

$$\bar{c}_n = \langle |W[h](a,b)| \rangle_b \tag{2.21}$$

The mean of the coefficient on each level is calculated. Then, the means versus the levels are plotted on a log-log plot. A standard linear regression to this plot will have a slope $H_{fBm} + \frac{1}{2}$, and the spectral index is found by $\beta = 2H_{fBm} + 1$ [6].

3.0 NUMERICAL ANALYSIS SCHEME

3.1 EVALUATION OF ALGORITHMS

3.1.1 Discrete $1/f^{\beta}$ Process Generation

The first step in the analysis was the generation of a $1/f^{\beta}$ fractal process. Li, et al proposed a method to create a filter of fractional order for generating fBm fractal processes by stochastically fractional differential equations [30, 42, 44]. Kasdin extended this method for a generalized fractional filter inclusive of fGn and fBm signals, or $1/f^{\beta}$ processes [43]. This method was implemented for this numerical analysis of $1/f^{\beta}$ processes. The transfer function of the fractional system that follows the power law of β is given by

$$h(n) = \frac{\Gamma(\beta/2 + n)}{n!\Gamma(\beta/2)} \tag{3.1}$$

which can be calculated by the following recursive algorithm, where the initial value $h(0) = 1$.

$$h(n) = \left(\frac{\beta}{2} + n - 1\right) \frac{h(n) - 1}{n} \tag{3.2}$$

Finally, the realization of the process $x(n)$ is found by the convolution operation

$$x(n) = w(n) * h(n) \tag{3.3}$$

where $w(n)$ is randomly generated Gaussian white noise.

3.1.2 Numerical Analysis of Simulated Time Series

The basis of this computational evaluation is the generation of $1/f^{\beta}$ power law processes. For completeness, β is calculated for all possible Hurst exponents in fGn and fBm classes for a total range $-1 \leq \beta \leq 3$. This is inclusive of fractional Gaussian noise and fractional Brownian motion processes for $0 < H < 1$. However, the anti-correlated fGn ($\beta < 0$) and anti-persistent fBm ($\beta > 2$) regime signals are not be a matter of serious consideration in regard to physiological processes. The methods are evaluated over a range of time series lengths in order to observe the relationship between signal length and calculation accuracy for each fractal method. Given the length limitations of previously recognized physiological data sets, time series lengths of 50, 100, 200, 400, 600, 800, 1,000, 2,500, 5,000, 7,500, and 10,000 points are simulated. Given the stochastic nature of these processes, it is important determine a convergent value on which each technique calculates β. The procedure of signal generation and calculation is implemented in a Monte Carlo scheme, where each realization is repeated 1,000 times. In each iteration for a set signal length, the time series is normalized and evaluated by each of the methods. Next, and a unit mean offset is added, and this signal reevaluated by each method. Then the mean of the series is subtracted from the offset series, resulting in a zero mean signal, and reevaluated. An overview of example signals from each of these considered cases is given in Figure 3.1. These three cases are calculated for each signal length for 1,000 realizations, and the mean value of β from each estimation is calculated. This computational scheme is the basis of the theoretical qualification of the fractal characterization algorithms, with strong consideration of the two recognized constraints of signal length and mean. Importantly, each iteration is carried out for the same realization of randomly generated $1/f^{\beta}$ process. Over the range of β, processes of the given length are generated for $[-1, 3]$ incremented by 0.01.

3.1.3 Numerical Analysis of Stride Interval Time Series

Lastly, the publshed data sets are re-examined. First considered are right foot gait stride interval time series from normal subjects, consistent with previous investigation by Hausdorff,

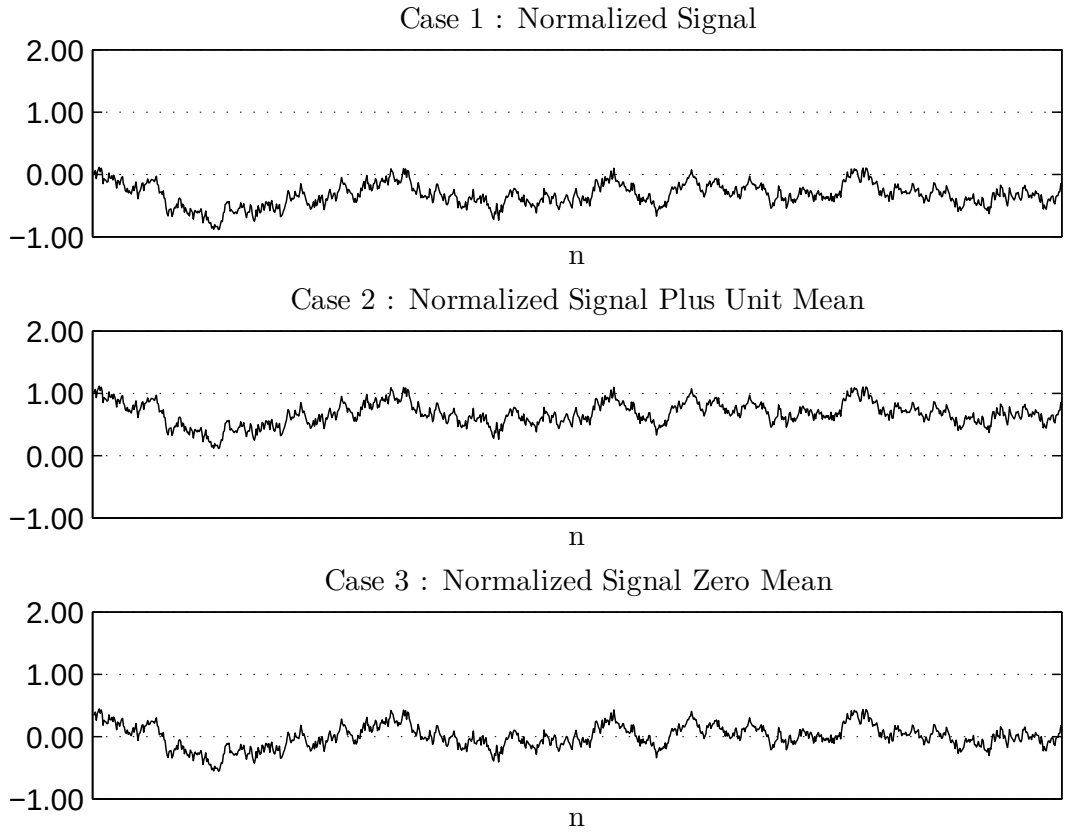

Figure 3.1: Example Simulated Time Series, Cases 1 - 3 ($\beta = 1.5$)

et al in the study of long range correlations in stride interval fluctuations [4] and reconsidered by Deligieneras [23]. Each of 10 healthy adult subjects walked at a self selected slow, normal, and fast pace, providing 30 total time series. This study, henceforth referred to as Study I, implemented a power spectral analysis and DFA to find β and α respectively [4] to qualify and compare each method for fractal dynamics in gait. An example healthy long length time series and power spectrum provided by this study is shown in Figure 3.2.

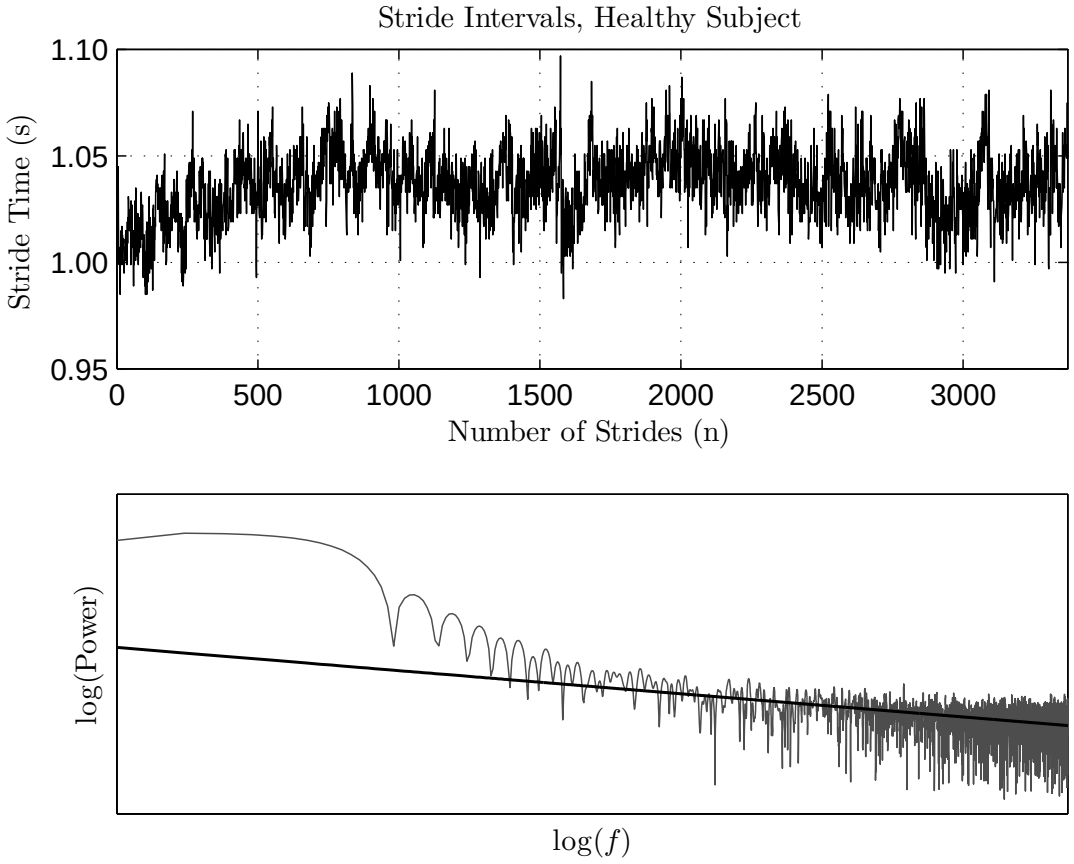

Figure 3.2: Stride Interval Time Series and PSD of Healthy Subject, Study I. $\beta = 0.60$

The mean time series length for the ten healthy control subjects is 3,179 points. Given the signals' significant length, these are considered to be a basis set for evaluating the algorithm performance under sufficiently long signal lengths. For consistency with the previous investigations, only the first 2,048 points are used for calculation.

The second set comes from an investigation of gait dynamics in neurodegenerative diseases. The data was obtained by Haussdorf, et al in investigations of healthy and pathological correlations in stride interval time series [4, 15, 16]. The signal lengths are considerably constrained due to the physical limitations of the subject. An example pathological (ALS) short length time series and power spectrum provided by this study is shown in Figure 3.3. In the investigation henceforth referred to as Study II, α was calculated by DFA. To again retain consistency with the previous investigation, only the right foot stride interval time series is considered for calculation. Listed in Table 3.1 are the total number and mean length of time series for each of the cases of pathology and the control. The evaluation here is aimed to demonstrate the algorithm performance in the regime of short time series.

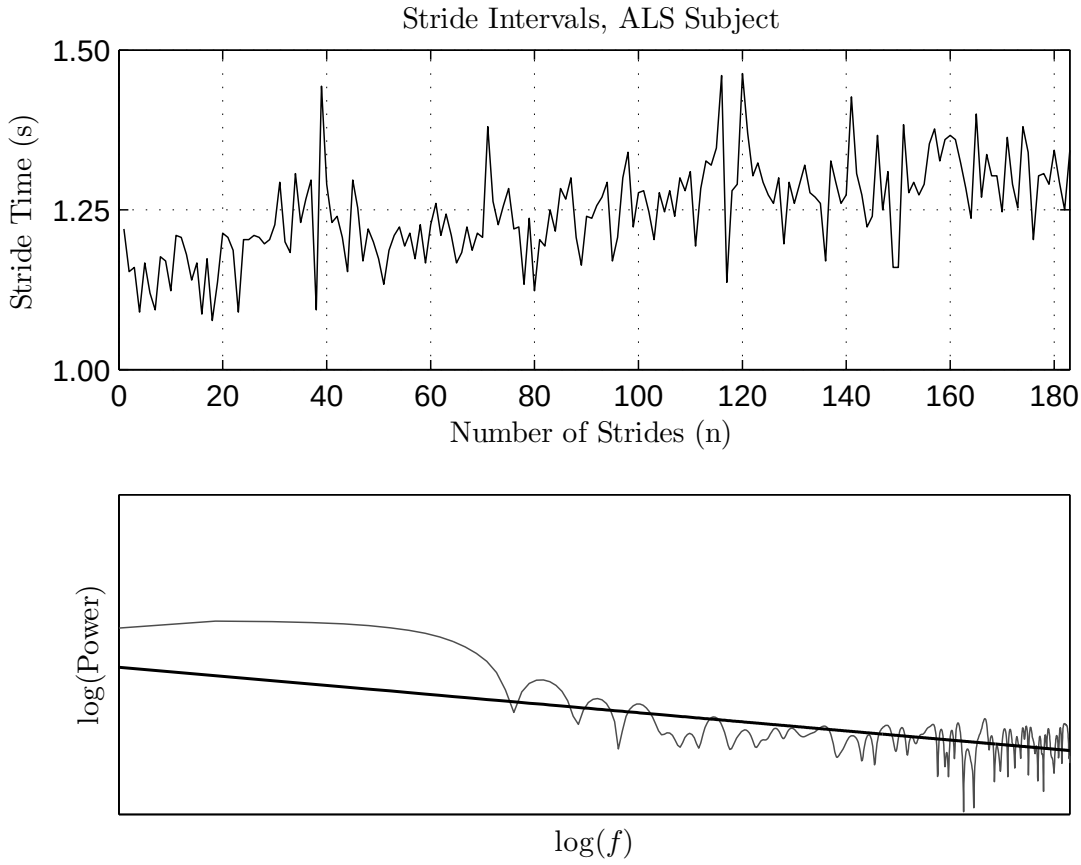

Figure 3.3: Stride Interval Time Series and PSD of ALS Subject, Study II. $\beta = 0.45$

Table 3.1: Number of Time Series and Mean Length, Study II. ALS = Amyotrophic Lateral Sclerosis, HD = Huntington's Disease, PD = Parkinson's Disease, CO = Control

	ALS	**HD**	**PD**	**CO**
Number of Series	13	20	15	16
Mean Length	196	242	184	255

4.0 RESULTS

Presented in this section are the results of the numerical analysis scheme. Secondly, the results from the evaluation of the published physiological data sets of long time series from healthy individuals and shorter time series of neurodegenerative disease subjects are examined. From the results of the numerical analysis, this thesis seeks to indicate which of the estimators can most effectively evaluate fractal nature of the physiological time series under the various constraints. The importance of accurately measuring β of the physiological time series is also presented in this section, so the calculations of the physiological data are compared with previously published results.

4.0.4 Overall Theoretical Performance

Considered first is the estimation accuracy of the algorithms for $-1 \leq \beta \leq 3$. This presents the performance of the general scheme, which calculates the mean spectral index β of $1,000$ random fractal signals of lengths varying from 50 to $10,000$ points. This is under a normalized condition. Shown are the mean-square error (MSE) of the estimators on the range $-1 \leq \beta \leq 3$ for signal lengths of of 100 and 10,000 points in Figure 4.1(a) and (b), respectively.

The results of our analysis indicate that some estimators are indeed not class independent. Figure 4.1(a) shows the MSE of the estimators on the range $-1 \leq \beta \leq 3$ for signal length of 100. For a short signal length, it is clear that bdSWV and dispersional analysis estimators are fBm and fGn class dependent, respectively. The bdSWV method exhibits very high MSE for the fGn class ($\beta < 1$) and dispersional analysis shows high MSE for all fBm class signals

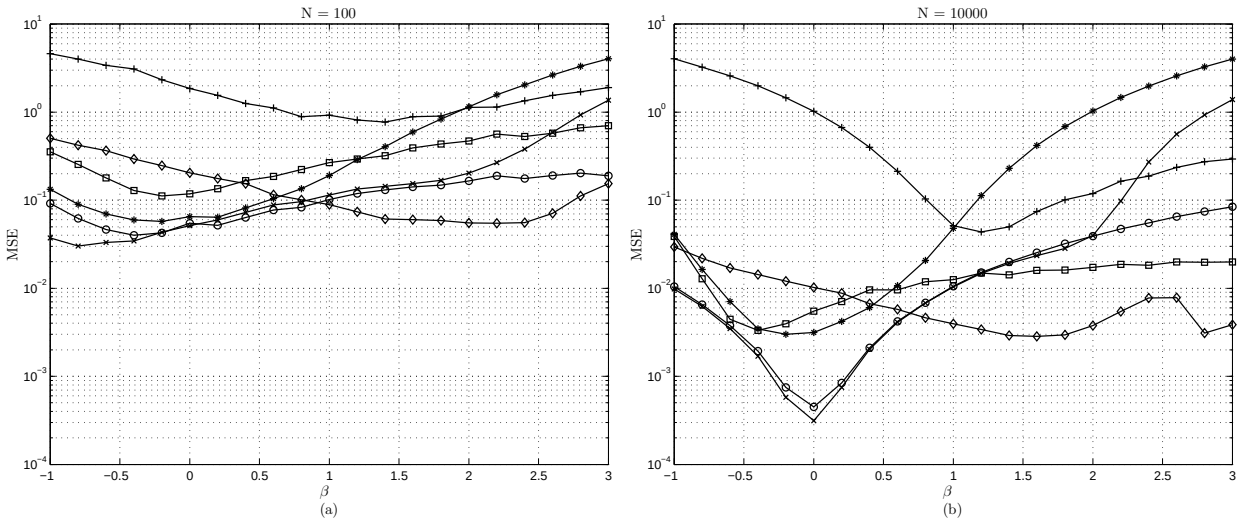

Figure 4.1: MSE vs β: (a) N = 100 points, (b) N = 10,000 points. $\Diamond$ AWC, + bdSWV, $\Box$ DFA, $*$ Disp, $\times$ PSD, $\circ$ ${}^{low}PSD_{we}$.

($\beta > 1$). Similar error in the fGn class is noted for the AWC method, and the error decreases for $\beta > 1$. DFA exhibits relatively high MSE values for both fBm and fGn processes with a relatively flat profile on this range. However, DFA demonstrates slightly greater accuracy than AWC method for signals close to white Gaussian fGn signals. Both power spectral density methods, the periodogram (PSD) and the modified method ${}^{low}PSD_{we}$ show quite consistent accuracy for all signal classes with a relatively flat MSE profile across the range of β. Interestingly, for short signal lengths, the basic periodogram (PSD) method is more accurate than the ${}^{low}PSD_{we}$ method. However, the MSE of the PSD increases significantly for persistent fBm type signals ($\beta > 2$).

Considering the case of long time series length of 10,000 points given in Figure 4.1(b) it is clear that the bdSWV method has significantly high MSE for all fGn class signals ($\beta < 1$). Similarly, dispersional analysis demonstrates high MSE for all fBm class signals ($\beta > 1$). AWC shows relatively consistent MSE for both classes, though the MSE decreases as the signal type approaches Brownian motion ($\beta = 2$). There is though an observable MSE

increase for persistent fBm signals. DFA similarly demonstrates class independent behavior, with lower MSE for fGn class signals. Again in the long signal length case, DFA indicates DFA exhibits a relatively consistent MSE in both the fGn and fBm class. Both power spectral density methods, the periodogram (PSD) and the modified method ${}^{low}PSD_{we}$ demonstrate similar MSE, which is loewst for white Gaussian noise fGn processes. Higher MSE is observed for fBm class signals, though the error is not as high as in the class dependent dispersional and bdSWV methods. The modified PSD method shows higher accuracy than the standard periodogram for persistent fBm type signals ($\beta > 2$).

Given the clear relationship of the MSE and the signal length, examined next is the MSE value over a range of signal lengths. Each value is the 1,000 realization ensemble mean MSE for the given length. For conciseness, anti-correlated fGn ($\beta = -1$) and persistent fBm ($\beta = 3$) evaluations are excluded. Shown in Figure 4.2(a) is the mean-square error (MSE) of the estimators on the range $50 \leq N \leq 10,000$ for white Gaussian noise fGn signals of $\beta = 0$.

Expectedly, for the white Gaussian noise case of fGn class signals $\beta = 0$, the MSE of the bdSWV method is high regardless of signal length. The MSE for dispersional analysis decreases as signal length increases, and at long signal length is among of the most accurate estimators for this signal class. Interestingly, DFA shows diminishing returns in accuracy beyond $N = 1,000$. AWC consistently shows increasing accuracy as signal length increases. For the white Gaussian case of fGn signals, the power spectral density methods again exhibit the lowest overall MSE which decreases for greater signal length.

The mean-square error (MSE) of the estimators on the range $50 \leq N \leq 10,000$ is observed in the critical case of the boundary of fGn and fBm signals for $1/f^{\beta}$ processes of $\beta = 1$. Here, it is expected to see that regardless of signal length, both class dependent methods bdSWV and dispersional analysis exhibit crossover and a similar order of MSE. DFA shows initially high MSE that decreases as signal length increases, though again with quickly diminishing returns. The power spectral density methods show a similar profile. AWC again shows increasing accuracy as the length is increased. For shorter length signals cases, the MSE of AWC, DFA, and spectral methods are clustered closely together.

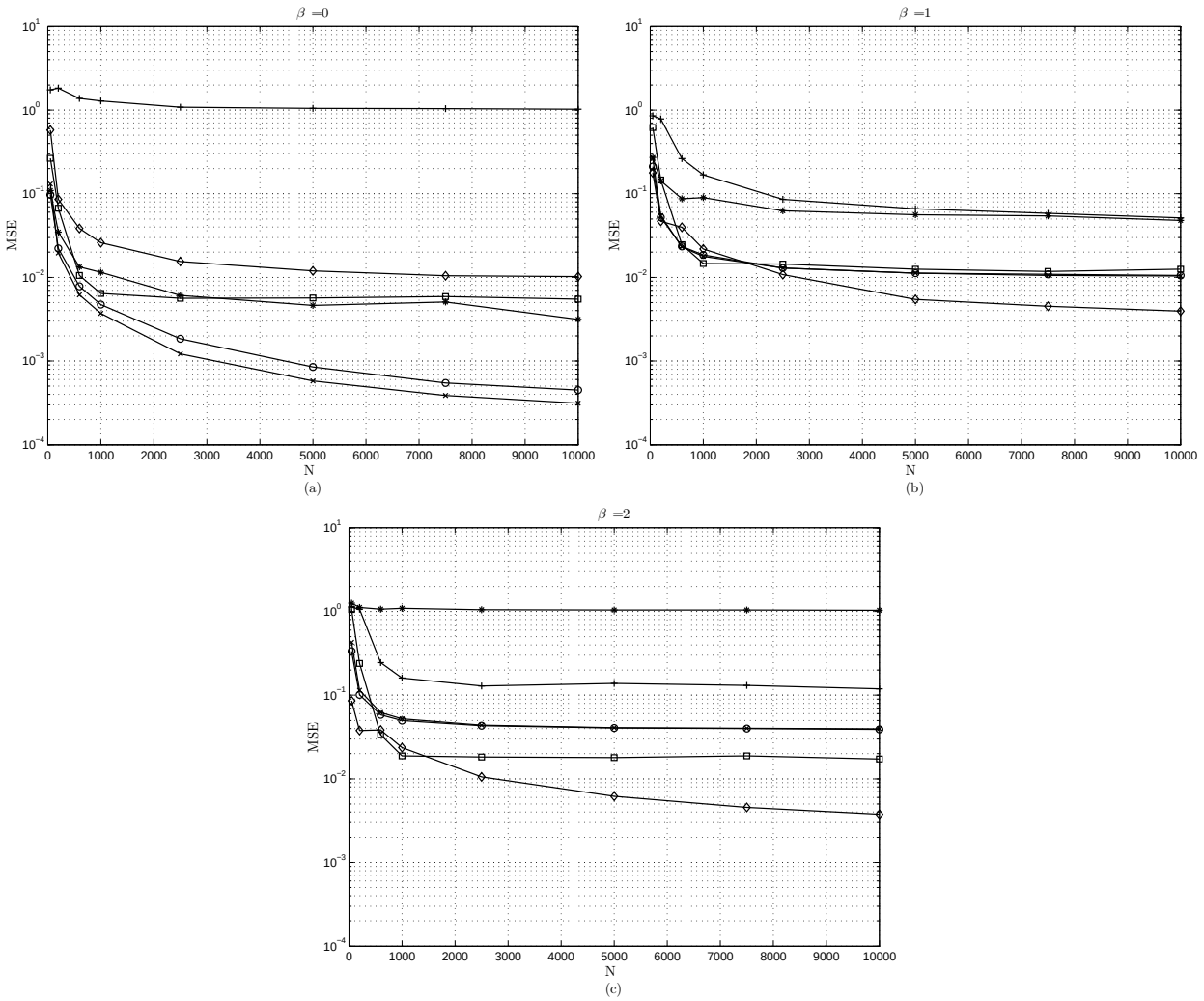

Figure 4.2: MSE vs n: (a) $\beta = 0$, (b) $\beta = 1$, (c) $\beta = 2$ $\Diamond$ AWC, + bdSWV, $\Box$ DFA, $*$ Disp, $\times$ PSD, $\circ$ $^{low}PSD_{we}$

The third case consideration is the MSE versus length for Brownian motion fBm signals of $\beta = 2$. For the Brownian motion process indicative of the fBm class, the MSE of dispersional analysis is high regardless of signal length, indicating its class dependence. The MSE of bdSWV is lower than in the fGn class, though it is still significantly greater than other methods. DFA reaches its maximum accuracy at $N = 1,000$ points. AWC exhibits the

sharpest drop off in error of all methods, and regardless of signal length has generally the lowest error for Brownian motion fBm class signals. The spectral methods show low MSE for very short time series, but quickly diminishing returns for signals greater than 1,000 points.

Considering the class dependence of the bdSWV and dispersional analysis methods, subsequent observations of the results will not consider findings for these methods. This is in the interest of determining a robust class independent estimator. Accordingly, ${}^{low}PSD_{we}$ is considered class independent for its modifications which allow a more accurate estimation of fBm processes than the unmodified periodogram method. In conclusion, further elaborations on the MSE, mean error (ME), and standard deviation (SD) of techniques will consider DFA, ${}^{low}PSD_{we}$, and AWC.

Figure 4.3 shows the mean-square error (MSE) of the estimators DFA, ${}^{low}PSD_{we}$, and AWC on the range $-1 \leq \beta \leq 3$ for signal length of 100, 600, 2,500, and 10,000. For the two short series sets ($N = 100$, $N = 600$), all methods exhibit a relatively consistent profile of MSE over the entire range of β. For short time series, AWC is most accurate in the fBm class, and ${}^{low}PSD_{we}$ is most accurate in the fGn class. DFA is generally less accurate than AWC and ${}^{low}PSD_{we}$. Though DFA may be more accurate than AWC at estimating a white Gaussian fGn process, the accuracy of ${}^{low}PSD_{we}$ is still preferable. A similar observation can be made in subsequently longer time series of length 600, 2,500, and 10,000. DFA shows preferable performance to AWC near white Gaussian noise, and here the accuracy of ${}^{low}PSD_{we}$ is always favorable. An important characteristic of AWC is its relatively flat MSE over the range of β for all signal lengths. A notable increase in MSE exists for ${}^{low}PSD_{we}$ in the fBm class as the length is increased, due to the effects of more low frequency content in these signals.

The definition of MSE necessarily combines the bias and variance into one value. To distinguish the individual effects of bias and variance in the notion of the estimators' MSE on this range, the bias (mean error) and variance (standard deviation) will be examined separately in the following figures. Figure 4.4 shows the mean error (ME) of AWC, ${}^{low}PSD_{we}$, and DFA on the range $-1 \leq \beta \leq 3$ for signal lengths of 100, 600, 2,500, and 10,000.

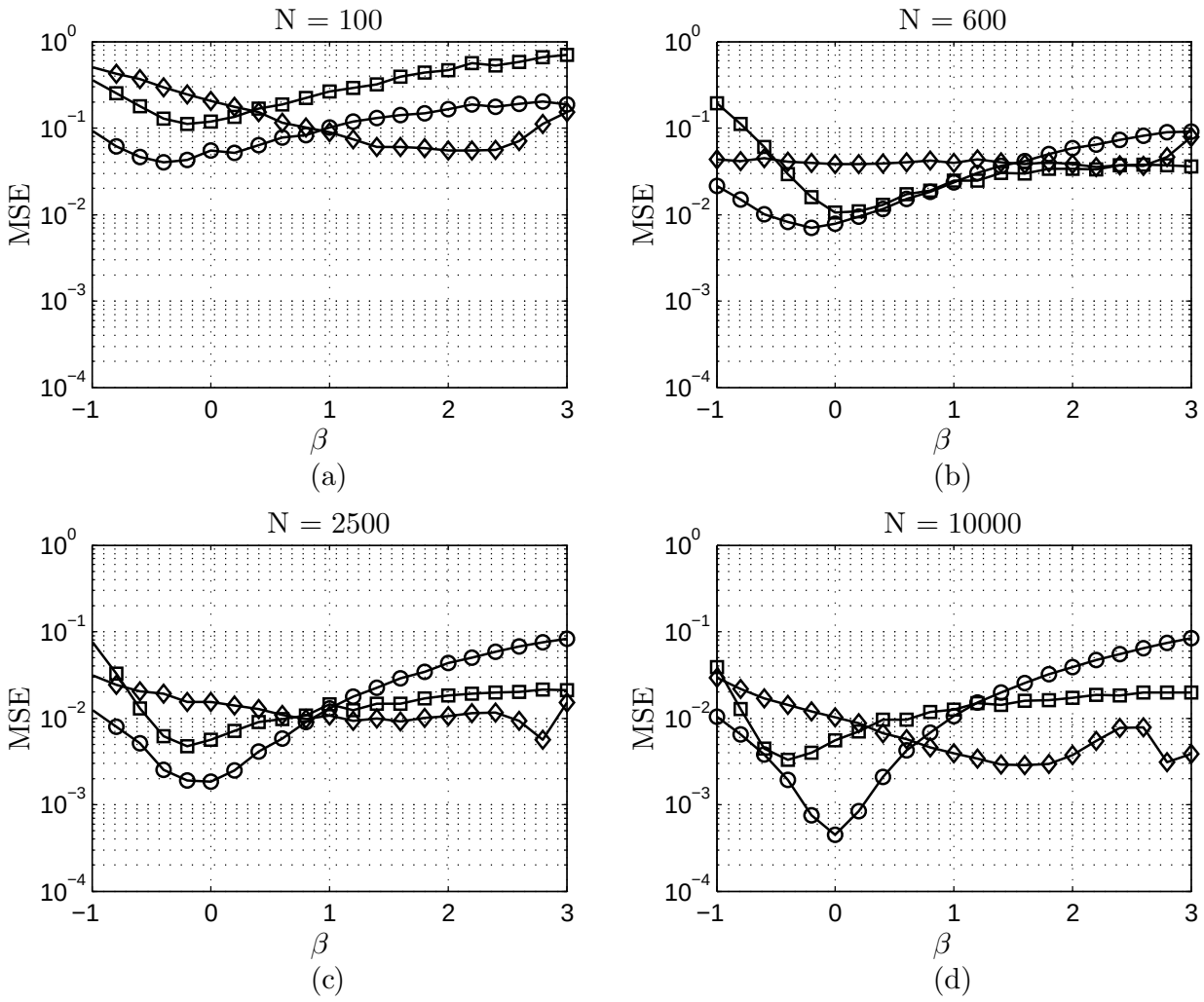

Figure 4.3: MSE vs β: (a) n = 100 points, (b) n = 600 points, (c) n = 2,500 points, (b) n = 10,000 points. $\Diamond$ AWC, $\square$ DFA, $\circ$ ${}^{low}PSD_{we}$

Figure 4.4 indicates that for short time series, MSE of AWC is largely influenced by bias. This effect is diminished in the fBm regime. The mean error of DFA is lower than ${}^{low}PSD_{we}$ and AWC for the fGn class. The MSE of DFA is consistently influenced by bias in the fBm range. ${}^{low}PSD_{we}$ exhibits less overall fluctuation, and estimation bias increases with β. This is likely due to the influence of more low frequency components when evaluating the linear

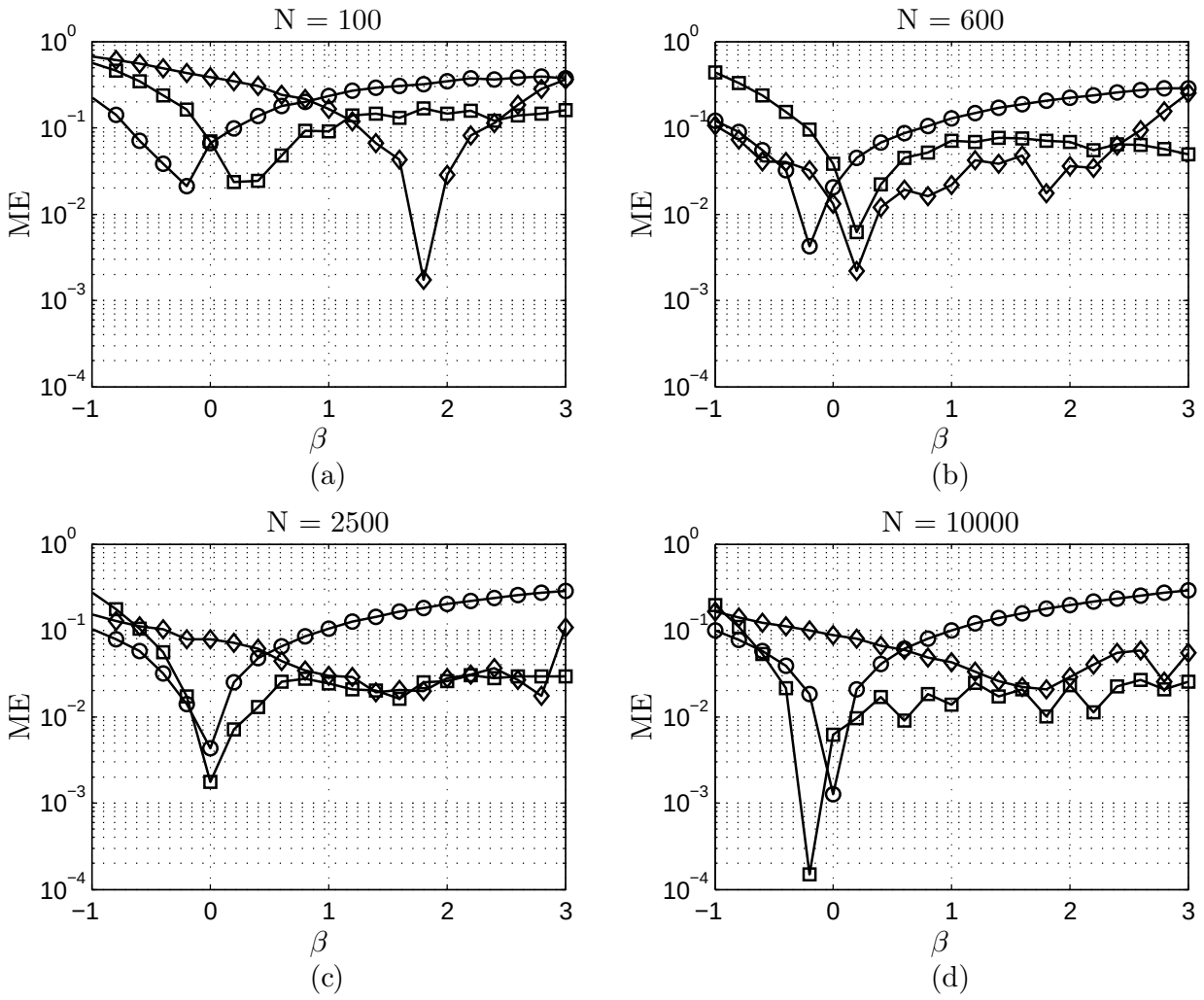

Figure 4.4: ME vs β. (a) N = 100 points, (b) N = 600 points, (c) N = 2,500 points, (b) N = 10,000 points. $\Diamond$ AWC, $\Box$ DFA, $\circ$ ${}^{low}PSD_{we}$.

regression of the power spectral density. For subsequently longer signal lengths of 600, 2,500, and 10,000, the bias effects on the MSE of DFA and AWC are comparable beyond $\beta = 0$.

Figure 4.5 shows the standard deviation (σ) of DFA, ${}^{low}PSD_{we}$, and AWC on the range $-1 \leq \beta \leq 3$ for signal length of 100, 600, 2,500, and 10,000. For short signal length, the standard deviation of DFA is significant. The standard deviation of ${}^{low}PSD_{we}$ and AWC are

very consistent on the range of β. ${}^{low}PSD_{we}$ shows the overall lowest standard deviation for both signal classes for all signal lengths. For longer signal lengths, the standard deviation profile of DFA is relatively unchanged. The profile of AWC is flat in each case, with increasing accuracy with signal length. DFA exhibits lower standard deviation than AWC for fGn class signals of length 600 and 2,500, though the accuracy of ${}^{low}PSD_{we}$ is still preferential.

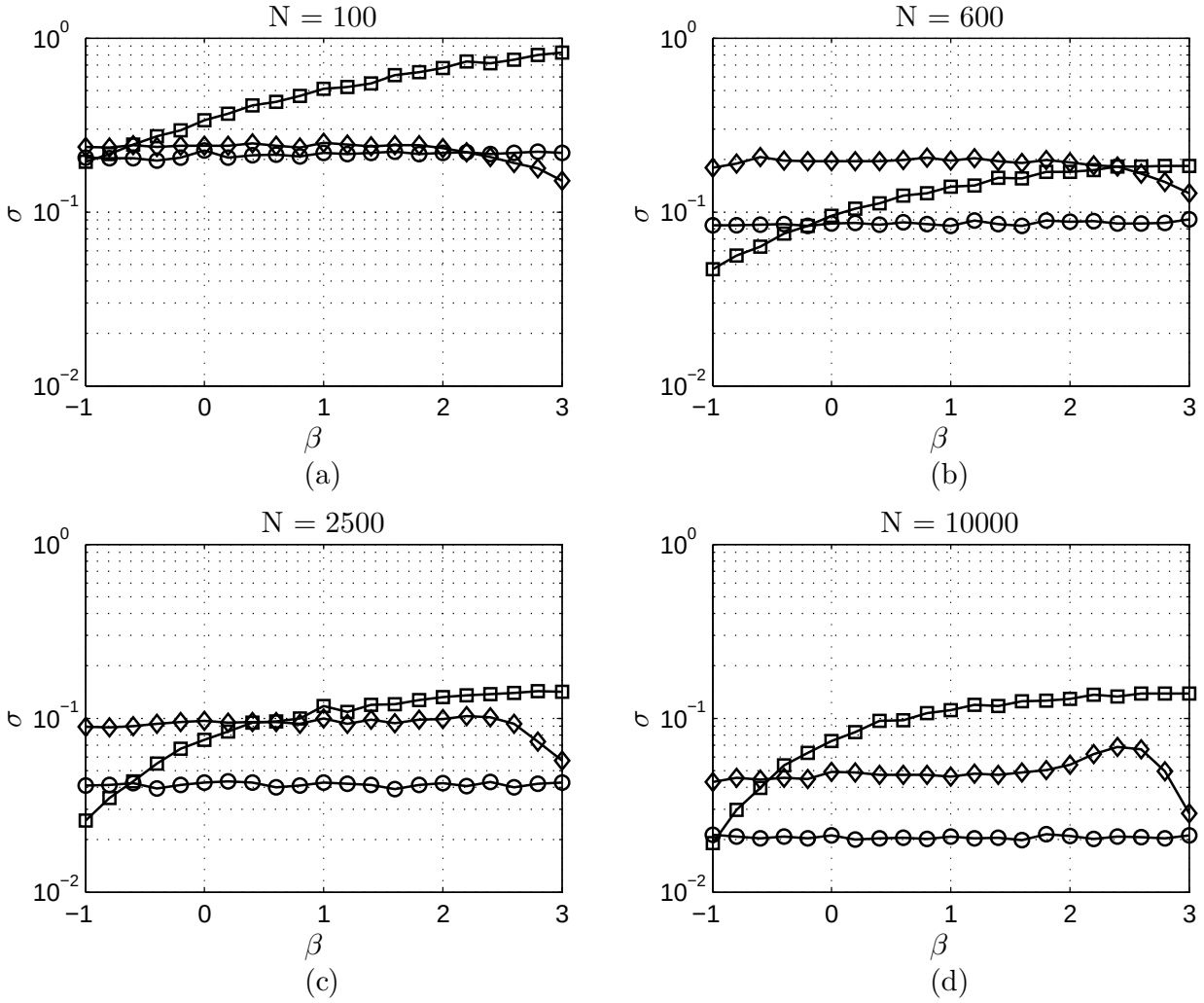

Figure 4.5: σ vs β: (a) N = 100 points, (b) N = 600 points, (c) N = 2,500 points, (d) N = 10,000 points. ◊ AWC, □ DFA, ○ ${}^{low}PSD_{we}$.

4.0.5 Effects of Nonzero Mean

4.0.5.1 Added Unit Mean Presented in this section are findings for realizations of the algorithms for the complete range $-1 \leq \beta \leq 3$. The results are evaluations on an extension of the previously described scheme where a the signal is normalized and unit mean is added. Figure 4.6 (a) and (b) show the mean-square error (MSE) of the estimators on the range $-1 \leq \beta \leq 3$ for biased signal length of 100 and 10,000, respectively.

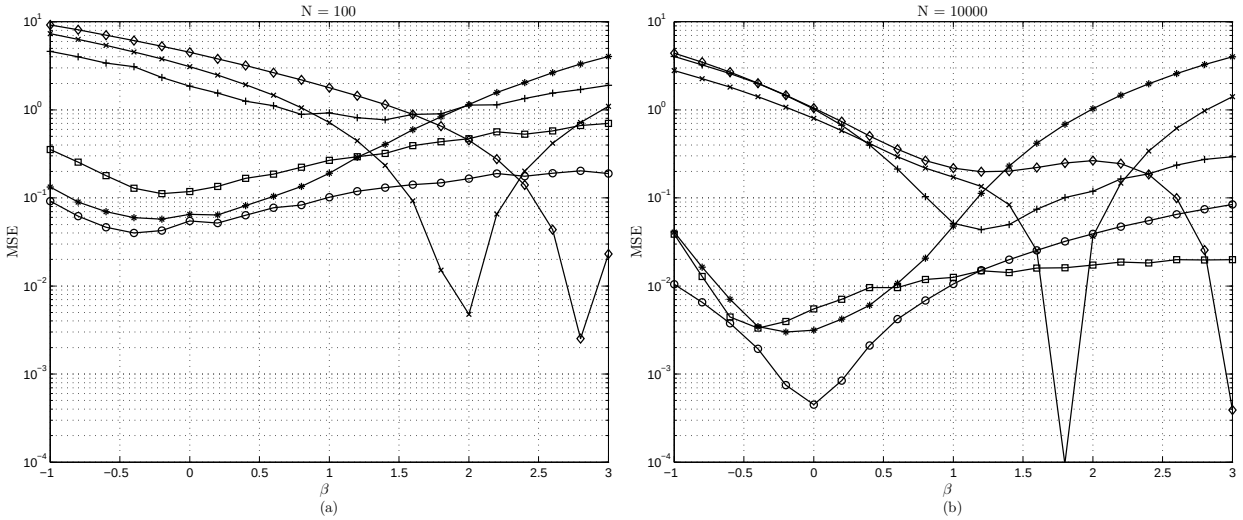

Figure 4.6: MSE vs β, unit mean: (a) N = 100 points, (b) N = 10,000 points. $\Diamond$ AWC, + bdSWV, $\Box$ DFA, $*$ Disp, $\times$ PSD, $\circ$ ${}^{low}PSD_{we}$

Compared to the original normalized signal condition shown in Figure 4.6, the additional unit mean affects only the MSE of the frequency and time-scale domain methods. The adjustments introduced to the power spectral density method by ${}^{low}PSD_{we}$ avoid the error effects of nonzero mean. It is critical to note that a significant DC component from a series mean will largely influence a low frequency range of the power spectral density, and subsequently the linear regression estimation for the spectral estimators. However, the constant unit mean has diminishing influence on increasingly non-stationary processes, and thus the effect is diminished as β increases. This observation is reflected in the findings of the dependence of the MSE on signal length with nonzero mean. Inaccuracy in the AWC

method is significantly influenced in the fGn class, and error is still generally present for all fGn and fBm class signals. The nonzero mean has no effect on the time domain methods.

4.0.5.2 Removal of Mean Finally observed is the estimation accuracy when the series mean is removed. These results are from the third extension of the numerical analysis scheme. From the second case where the signal is normalized and unit mean is added, the mean of the resulting signal is calculated and subtracted from the time series. Shown in Figure 4.7 (a) and (b) are the mean-square error (MSE) of the estimators on the range $-1 \leq \beta \leq 3$ for a zero mean signal length of of 100 and 10,000, respectively.

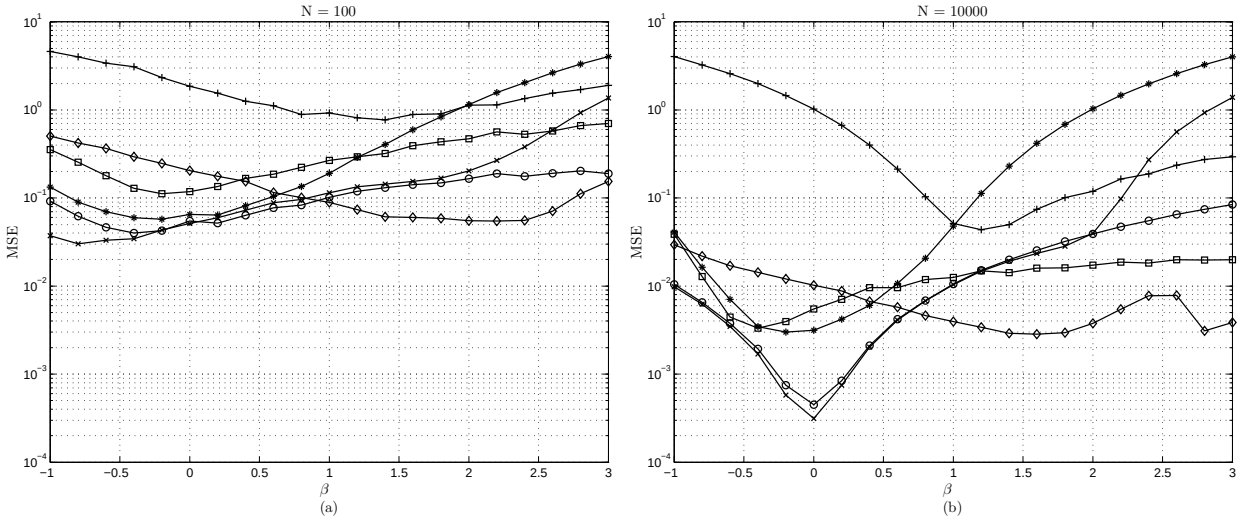

Figure 4.7: MSE vs β, zero mean: (a) N = 100 points, (b) N = 10,000 points. $\Diamond$ AWC, + bdSWV, $\Box$ DFA, $*$ Disp, $\times$ PSD, $\circ$ ${}^{low}PSD_{we}$

Figure 4.7 indicates that when the mean is removed by simply subtracting the mean value of the series, the estimation accuracy returns to the original profile. Thus, removing the series mean is valid to avoid errors in series estimation by methods which are sensitive. The original mean square error, mean error, and standard deviation profiles are realized when the series mean is removed and the series is reevaluated.

4.0.6 Gait Stride Interval Analysis

This section presents the results the application of these techniques to experimentally measured gait stride interval time series. To keep the analysis concise, the methods implemented were those of the lowest MSE from each domain class. Thus, β was calculated by DFA, ${}^{low}PSD_{we}$, and AWC. For the AWC calculation, the preprocessing step of mean removal is performed. For a thorough evaluation of Study I, β is calculated and converted to α by the relationship $\alpha = \frac{\beta+1}{2}$. For clarity, these calculated values of β and α are presented separately in Table 4.1, showing the values (*mean* $\pm$ *standard deviation*) from the study and our calculations for DFA, ${}^{low}PSD_{we}$, and AWC.

Table 4.1: A Comparative Analysis of the Algorithms for Time Series, Study I

		β			α		
		Slow	**Normal**	**Fast**	**Slow**	**Normal**	**Fast**
Study I	DFA	0.96± 0.13	0.80± 0.07	0.94± 0.09	0.98± 0.07	0.90± 0.04	0.97± 0.05
	PSD	1.01± 0.15	0.81± 0.09	0.94± 0.07	1.01± 0.08	0.91± 0.05	0.97± 0.04
Analysis	DFA	0.93± 0.13	0.77± 0.15	0.94± 0.17	0.97± 0.07	0.88± 0.08	0.97± 0.09
	${}^{low}PSD_{we}$	0.73± 0.15	0.48± 0.09	0.62± 0.17	0.87± 0.08	0.74± 0.05	0.81± 0.09
	AWC	1.07±0.17	0.87±0.10	1.00± 0.18	1.03±0.09	0.94± 0.05	1.00± 0.09

Considered next are calculations for shorter time series of pathological gait conditions from Study II. Due to the physical limitations of the patients under investigation, the shortness of the time series length given in Table 3.1 is noted when considering the results of these calculations. Again, the spectral index β is calculated by DFA, ${}^{low}PSD_{we}$, and AWC and converted to the DFA scaling exponent α. The series mean has been removed for calculation by AWC. Table 4.2 shows the published and calculated values (*mean* $\pm$ *standard error*) of β and the corresponding of α for the calculations by DFA, ${}^{low}PSD_{we}$, and AWC methods.

Table 4.2: A comparative analysis of the algorithms for time series from Study II

		β				α			
		ALS	**HD**	**PD**	**CO**	**ALS**	**HD**	**PD**	**CO**
Study II	DFA	0.48±0.13	0.20±0.07	0.64±0.11	0.82±0.09	0.74±0.07	0.60±0.04	0.82±0.06	0.91±0.05
Analysis	DFA	0.66±0.13	0.37±0.12	0.52±0.16	0.60±0.10	0.83±0.07	0.68±0.06	0.76±0.08	0.80±0.05
	${}^{low}PSD_{we}$	0.56±0.08	0.26±0.09	0.39±0.11	0.49±0.05	0.78±0.04	0.63±0.05	0.70±0.06	0.74±0.03
	AWC	0.97±0.10	0.54±0.13	0.73±0.15	0.94±0.06	0.98±0.05	0.78±0.06	0.87±0.08	0.97±0.03

5.0 DISCUSSION

5.1 SIMULATED SIGNALS

From the results of the theoretical evaluation of these techniques, distinct limitations and benefits of each of the methods can be observed. When determining an appropriate technique to evaluate the fractal nature of a process, it is critical to consider the time series length, any apparent mean, and in some cases the range on which the process's spectral index might exist. It is therefore apparent from our analysis that making a conclusion about the fractal nature of short physiological time series can be quite tenuous. The nature of physiological data sets and their relationship to ideal $1/f^{\beta}$ profiles should be a significant consideration when drawing conclusions about the results of these analyses.

In the interest of determining class independent estimators, the dispersional and bdSWV methods are clearly not viable. Though developed for consideration of fGn and fBm class signals respectively, these methods can provide incorrect results for signals typical of physiological processes at $\beta = 1$. The recommendation to favor class independent methods is to effectively reduce the burden of determining the signal class before evaluation. DFA is a candidate, as it indicates no preferential performance in either class. Additionally, the evaluation is unaffected by a non-zero series mean. However, the results for DFA have significantly large MSE and standard deviation for short time series [29]. It is apparent that DFA has little utility for short time series, and exbhibits diminishing returns in accuracy for longer series, as other investigations have observed [26, 29, 58].

A significant limitation of the frequency domain methods is the effect of low frequencies and DC on the accuracy of these methods. Indeed, a the critical property of fractal processes is that the power spectral density is not convergent for ($\omega = 0$), and this presents some problems for analysis [30]. However, removing DC and low frequency content from the spectrum risks destroying low frequency information, and thus some scale invariant features of the process. Additionally, the significantly lower MSE observed in the spectral methods for white Gaussian fGn processes is likely an artifact of the time series generation by the same principle [43]. Regardless, accurately estimating the properties of white Gaussian processes does not present any significant utility with respect to the interest of fractal characterization of physiological processes, where a simple autocorrelation analysis or Lilliefors test may suffice.

AWC has a more uniform performance for the range of fGn and fBm class signals. Though AWC was significantly affected by non-zero mean signals, this effect is corrected by the removal of the time series mean before evaluation. Unlike the modifications to spectral methods to eliminate ill-fitting due to DC or high frequency noise, this is a straightforward preprocessing step easily integrated with the main algorithm. This combination also provides intact frequency and scale dependent information of the series. DFA presents significant risk for short time series and provides no clear advantage in many instances, where ${}^{low}PSD_{we}$ can likely provide a more accurate complement to AWC analysis. In general, given these two primary constraints of non-zero mean and short time series in gait stride interval signals, AWC can provide uniformly accurate characterization for short and long biased data series. Regardless, discretion of the desired precision and accuracy, illustrated by the mean error and standard deviation, is encouraged in all applications. Generally, the MSE of all estimators indicate that AWC is a generally robust method, consistent under many circumstances and favorable especially under conditions of physiological interest.

5.2 STRIDE INTERVAL TIME SERIES

The analysis of the physiologically extracted time series provides perhaps the most significant indication of the applicability of these methods in a physiological setting. Table 4.1 shows the fractal characterizations for long time series of ten healthy adults walking at self selected paces. In these time series, the mean amplitude is 0.2025 and the mean of the series is 1.1481, indicative of the inherent non-zero mean offset. The effects of these signal characteristics are observed in our evaluation of these time series by DFA, ${}^{low}PSD_{we}$, and AWC. For the self selected slow, normal, and fast time series, the DFA and AWC methods evaluate a mean spectral index of 0.88 ± 0.15 and 0.98 ± 0.15 respectively. To validate this disparity, consider the results of the simulated time series for length of 100 and $\beta = 1$. The MSE of AWC is preferable in this instance, and is exemplified by observing the substantial standard deviation of DFA here. The underestimation of the spectral index here by ${}^{low}PSD_{we}$ is noted. Considering physiologically meaningful conclusions from the pathological gait data is more difficult given the inherently short length of the time series. These evaluations given by Table 4.2 show the findings for short time series of ALS, Huntington's Disease, Parkinson's Disease, and control subjects. For all series, the mean time series length is 190 points. The mean amplitude is 0.2788 and the mean of the series is 1.0866, again showing a non-zero mean offset. For pathological gait time series, more stationary fGn type characteristics may be expected. Given the MSE for β on the range of [0,1] for length of 100, the accuracy of DFA, AWC, and ${}^{low}PSD_{we}$ are generally comparable on the order of 10^{-1}. Table 4.2 still show disparity between each estimator, error largely affected by the time series length.

The drastic underestimation of the spectral index by the frequency domain based method is observed in both studies. To avoid error in the estimation introduced by noise, the ${}^{low}PSD_{we}$ necessitates removal of high frequency components of $1/8 * f_{max}$. The underestimation of the spectral index in the power spectrum indicates a greater effect of the high frequency content of the signal, so this adjustment did not quite nullify the effects of high

frequency biasing. Though the MSE of AWC and DFA are similar, the AWC method is similarly biased but has much lower standard deviation. DFA on this range again presents significant standard deviation. This highlights the critical concern of the application of DFA to pathological time series of short length. It is therefore concluded here that the results provided by AWC are more tenable.

It is clear that DFA and spectral methods in many instances require extensive modification to properly assess the data. It is seen that necessity of such modifications as a potentially hazardous burden which could render results incorrect and obfuscate interpretations. Indeed, in the proposal of these methods for gait stride interval analysis by Haussdorf, the window sizes and fitting ranges for DFA and the frequency range for the spectral method linear regression required significant scrutiny to achieve a desired result [4, 26]. In this case, the relationship between the scales of the significant physiological frequencies and noise frequencies can be inferred in a general sense. However, it is not always possible to make a clear distinction between noise and physiologically meaningful frequency content in all physiological and experimental settings. DFA similarly requires adjustment of the bounds of window size. This adjustment can significantly impacts the final calculation, and varies between applications depending on the amplitude of fluctuations in the chosen window. This would require specific specialization of this method for each application. The risks and burdens of specialization of these methods can be effectively reduced given the generally favorable performance AWC. It is noted that the only requirement to avoid errors in AWC is preprocessing the signal by subtracting the mean.

6.0 CONCLUSIONS AND FUTURE WORK

6.1 CONCLUSIONS

The objective of this study was to provide a comparative analysis of fractal characterization algorithms of $1/f^{\beta}$ time series with respect to physiological applications. Primarily, the numerical analysis allowed us to provide insight into the time series lengths and signal classes on which previously proposed algorithms returned acceptably accurate results. If fractal characteristics are of interest for some arbitrary physiological process, it is critical to choose a class independent algorithm with consistent accuracy and precision. When signal class is not given a priori or classification is not possible, these estimators have little utility. The evaluation of class dependent algorithms, bdSWV and dispersional analysis, has shown that they are not feasible in these applications. However, these are still relatively valid evaluations if a signal class can be determined. Once a process can be classified as fGn or fBm by a more robust consistent and accurate estimator such as AWC, a class specific estimator may provide a useful complementary analysis. In contrast to the findings under simulation, the inherent nature of experimentally derived physiological signals present further challenges in evaluating fractal properties. The sensitivity of power spectral methods to a non-zero mean and high frequency were observed, and necessitate the task of distinguishing the range of physiologically meaningful frequencies from noise. Similarly, the potential errors influenced in DFA from large local fluctuations in small window sizes were observed. The

general conclusion drawn from the simulated series indicated that AWC is numerically most reliable method to these time series without the burden of specific adjustments for each application. This numerical and corresponding gait stride interval physiological analyses provide a justifiable basis for the applications of AWC to a variety signals of interest for a more informative indicator of the fractal nature of these processes.

6.2 FUTURE WORK

This investigation uncovered many of the pitfalls of some methods of fractal time series analysis. Any recommendations of algorithm modification or development were out of the scope of this comparative assessment. For example, there are many ways in which modified spectral analysis and wavelet coefficient methods may be improved to more suitably characterize a physiological parameter of interest. In the interest of developing the general scheme, parameters of these algorithms were kept constant, but can certainly be optimized for specific applications. Also, this investigation focused on a simplified assumption of the complex phenomena of interest in that all processes are assumed to be monofractal. Presently it is unclear whether gait dynamics are monofractal. Though some multifractal analysis in physiology has been performed, it would be interesting to extend and refine this analysis to uncover potential multifractal dynamics in gait to better understand the specific mechanisms of disease and decline. Finally, it would be interesting to see more widespread adoption of fractal measures as a parameter in other investigations of nonlinear and nonstationary phenomena. It can be a useful measure in investigations of parameter spaces for pattern recognition problems in brain computer interfaces or dysphagia diagnostics, or as a basis for EEG complex brain network analysis. Finally, it seems that the fractal mathematics would be well suited to inform the development of more behaviorally accurate models of complex physiological systems. It would be useful to investigate the development of algorithms that can replicate the fractal process to predict future outcomes, to provide information of the subsequent trend of decline in a given system.

7.0 ACKNOWLEDGEMENT

First I would like to thank my parents Mark and Joyce for their unconditional love, support, and encouragement for me to pursue my love for studying science. I also owe much of my success and well-being throughout my studies to my sisters Kathleen and Lauren. Outside my immediate family, I have to thank those who believed in me and provided brilliant teaching, guidance, and learning opportunities. I have so much gratitude for the love and guidance of Professors Dr. Steven Levitan and Dr. Anna Balazs, whose support has had a profound impact on my life. I also must thank Professors Dr. Luis Chaparro and Dr. Amro El-Jaroudi for their enthusiastic and brilliant lectures, answering my questions, and providing much useful insight into the direction of this thesis. I also thank my friends and colleagues at the lab. My good friend Jason Larkin helped significantly throughout this research and study by offering advice, his immense technical knowledge, and often much needed levity. Finally, I thank my advisor Dr. Erivn Sejdić for his consistent guidance, patience and dedication to forming me into an effective researcher and engineer.

BIBLIOGRAPHY

[1] W. Tao, T. Liu, R. Zheng, and H. Feng, "Gait analysis using wearable sensors," *Sensors*, vol. 12, no. 2, pp. 2255–2283, 2012.

[2] V. T. Inman, "Human locomotion," *Canadian Medical Association Journal*, vol. 94, no. 20, p. 1047, 1966.

[3] J. M. Hausdorff, C. Peng, Z. Ladin, J. Y. Wei, and A. L. Goldberger, "Is walking a random walk? Evidence for long-range correlations in stride interval of human gait," *Journal of Applied Physiology*, vol. 78, no. 1, pp. 349–358, 1995.

[4] J. M. Hausdorff, P. L. Purdon, C. K. Peng, Z. Ladin, J. Y. Wei, and A. L. Goldberger, "Fractal dynamics of human gait: stability of long-range correlations in stride interval fluctuations," *Journal of Applied Physiology*, vol. 80, no. 5, pp. 1448–1457, 1996.

[5] A. Eke, P. Herman, J. Bassingthwaighte, G. Raymond, D. Percival, M. Cannon, I. Balla, and C. Ikrényi, "Physiological time series: distinguishing fractal noises from motions," *Pflügers Archiv European Journal of Physiology*, vol. 439, no. 4, pp. 403–415, 2000.

[6] A. Eke, P. Herman, L. Kocsis, and L. Kozak, "Fractal characterization of complexity in temporal physiological signals," *Physiological Measurement*, vol. 23, no. 1, p. R1, 2002.

[7] L. Glass, "Synchronization and rhythmic processes in physiology," *Nature*, vol. 410, no. 6825, pp. 277–284, 2001.

[8] R. W. Glenny, H. T. Robertson, S. Yamashiro, and J. B. Bassingthwaighte, "Applications of fractal analysis to physiology," *Journal of Applied Physiology*, vol. 70, no. 6, pp. 2351–2367, 1991.

[9] A. L. Goldberger and B. J. West, "Fractals in physiology and medicine." *The Yale Journal of Biology and Medicine*, vol. 60, no. 5, p. 421, 1987.

[10] H. V. Huikuri, T. H. Mäkikallio, K. J. Airaksinen, T. Seppänen, P. Puukka, I. J. Räihä, and L. B. Sourander, "Power-law relationship of heart rate variability as a predictor of mortality in the elderly," *Circulation*, vol. 97, no. 20, pp. 2031–2036, 1998.

[11] H. V. Huikuri, T. H. Mäkikallio, C. K. Peng, A. L. Goldberger, U. Hintze, M. Møller *et al.*, "Fractal correlation properties of RR interval dynamics and mortality in patients with depressed left ventricular function after an acute myocardial infarction," *Circulation*, vol. 101, no. 1, pp. 47–53, 2000.

[12] P. C. Ivanov, L. A. N. Amaral, A. L. Goldberger, S. Havlin, M. G. Rosenblum, Z. R. Struzik, and H. E. Stanley, "Multifractality in human heartbeat dynamics," *Nature*, vol. 399, no. 6735, pp. 461–465, 1999.

[13] C. K. Peng, S. Havlin, H. E. Stanley, and A. L. Goldberger, "Quantification of scaling exponents and crossover phenomena in nonstationary heartbeat time series," *Chaos: An Interdisciplinary Journal of Nonlinear Science*, vol. 5, no. 1, pp. 82–87, 1995.

[14] J. M. Hausdorff, L. Zemany, C. K. Peng, and A. L. Goldberger, "Maturation of gait dynamics: stride-to-stride variability and its temporal organization in children," *Journal of Applied Physiology*, vol. 86, no. 3, pp. 1040–1047, 1999.

[15] J. M. Hausdorff, A. Lertratanakul, M. E. Cudkowicz, A. L. Peterson, D. Kaliton, and A. L. Goldberger, "Dynamic markers of altered gait rhythm in amyotrophic lateral sclerosis," *Journal of Applied Physiology*, vol. 88, no. 6, pp. 2045–2053, 2000.

[16] J. M. Hausdorff, S. L. Mitchell, R. Firtion, C. K. Peng, M. E. Cudkowicz, J. Y. Wei, and A. L. Goldberger, "Altered fractal dynamics of gait: reduced stride-interval correlations with aging and Huntington's disease," *Journal of Applied Physiology*, vol. 82, no. 1, pp. 262–269, 1997.

[17] K. Sharma, J. Kent-Braun, S. Majumdar, Y. Huang, M. Mynhier, M. Weiner, and R. Miller, "Physiology of fatigue in amyotrophic lateral sclerosis," *Neurology*, vol. 45, no. 4, pp. 733–740, 1995.

[18] K. R. Sharma and R. G. Miller, "Electrical and mechanical properties of skeletal muscle underlying increased fatigue in patients with amyotrophic lateral sclerosis," *Muscle & nerve*, vol. 19, no. 11, pp. 1391–1400, 1996.

[19] O. Blin, A.-M. Ferrandez, and G. Serratrice, "Quantitative analysis of gait in parkinson patients: increased variability of stride length," *Journal of the neurological sciences*, vol. 98, no. 1, pp. 91–97, 1990.

[20] J. B. Bassingthwaighte, "Physiological heterogeneity: fractals link determinism and randomness in structures and functions," *Physiology*, vol. 3, no. 1, pp. 5–10, 1988.

[21] J. B. Bassingthwaighte and R. P. Bever, "Fractal correlation in heterogeneous systems," *Physica D: Nonlinear Phenomena*, vol. 53, no. 1, pp. 71–84, 1991.

[22] T. Chau, "A review of analytical techniques for gait data. part 1: fuzzy, statistical and fractal methods," *Gait & Posture*, vol. 13, no. 1, pp. 49–66, 2001.

[23] D. Delignieres and K. Torre, "Fractal dynamics of human gait: a reassessment of the 1996 data of Hausdorff et al." *Journal of Applied Physiology*, vol. 106, no. 4, pp. 1272–1279, 2009.

[24] S. M. Bruijn, D. J. Bregman, O. G. Meijer, P. J. Beek, and J. H. van Dieën, "Maximum Lyapunov exponents as predictors of global gait stability: A modelling approach," *Medical Engineering & Physics*, vol. 34, no. 4, pp. 428–436, 2012.

[25] D. Delignières, M. Fortes, G. Ninot *et al.*, "The fractal dynamics of self-esteem and physical self," *Nonlinear Dynamics in Psychology and Life Sciences*, vol. 8, pp. 479–510, 2004.

[26] D. Delignieres, S. Ramdani, L. Lemoine, K. Torre, M. Fortes, and G. Ninot, "Fractal analyses for short time series: a re-assessment of classical methods," *Journal of Mathematical Psychology*, vol. 50, no. 6, pp. 525–544, 2006.

[27] S. Havlin, S. Buldyrev, A. Goldberger, R. Mantegna, S. Ossadnik, C. Peng, M. Simons, and H. Stanley, "Fractals in biology and medicine," *Chaos, Solitons & Fractals*, vol. 6, pp. 171–201, 1995.

[28] S. Bruijn, O. Meijer, P. Beek, and J. Van Dieën, "Assessing the stability of human locomotion: a review of current measures," *Journal of The Royal Society Interface*, vol. 10, no. 83, 2013.

[29] R. M. Bryce and K. B. Sprague, "Revisiting detrended fluctuation analysis," *Scientific Reports*, vol. 2, 2012.

[30] M. Li, "Fractal time seriesa tutorial review," *Mathematical Problems in Engineering*, vol. 2010, 2009.

[31] B. B. Mandelbrot and J. W. Van Ness, "Fractional brownian motions, fractional noises and applications," *SIAM review*, vol. 10, no. 4, pp. 422–437, 1968.

[32] B. B. Mandelbrot, "Self-affine fractals and fractal dimension," *Physica Scripta*, vol. 32, no. 4, p. 257, 1985.

[33] J. W. Kantelhardt, S. A. Zschiegner, E. Koscielny-Bunde, S. Havlin, A. Bunde, and H. E. Stanley, "Multifractal detrended fluctuation analysis of nonstationary time series," *Physica A: Statistical Mechanics and its Applications*, vol. 316, no. 1, pp. 87–114, 2002.

[34] C. K. Peng, S. Havlin, J. M. Hausdorff, J. E. Mietus, H. E. Stanley, and A. L. Goldberger, "Fractal mechanisms and heart rate dynamics: long-range correlations and their breakdown with disease," *Journal of Electrocardiology*, vol. 28, pp. 59–65, 1995.

[35] M. F. Shlesinger, "Fractal time and 1/f noise in complex systems," *Annals of the New York Academy of Sciences*, vol. 504, no. 1, pp. 214–228, 1987.

[36] P. Bak and K. Chen, "Self-organized criticality," *Scientific American*, vol. 264, no. 1, 1991.

[37] M. S. Taqqu, V. Teverovsky, and W. Willinger, "Estimators for long-range dependence: an empirical study," *Fractals*, vol. 3, no. 04, pp. 785–798, 1995.

[38] G. Rangarajan and M. Ding, "Integrated approach to the assessment of long range correlation in time series data," *Physical Review E*, vol. 61, no. 5, p. 4991, 2000.

[39] W. Rea, L. Oxley, M. Reale, and J. Brown, "Estimators for long range dependence: an empirical study," *arXiv:0901.0762*, 2009.

[40] J. Beran, *Statistics for Long-Memory Processes, Monographs on Statistics and Applied Probability vol. 61.* Chapman and Hall, New York, 1994.

[41] M. Li and S. Lim, "Power spectrum of generalized Cauchy process," *Telecommunication Systems*, vol. 43, no. 3-4, pp. 219–222, 2010.

[42] ——, "A rigorous derivation of power spectrum of fractional gaussian noise," *Fluctuation and Noise Letters*, vol. 6, no. 04, pp. C33–C36, 2006.

[43] N. J. Kasdin, "Discrete simulation of colored noise and stochastic processes and 1/f power law noise generation," *Proceedings of the IEEE*, vol. 83, no. 5, pp. 802–827, 1995.

[44] M. Li and S. Chen, "Fractional gaussian noise and network traffic modeling," in *Proceedings of WSEAS International Conference. Mathematics and Computers in Science and Engineering*, no. 8. World Scientific and Engineering Academy and Society, 2009.

[45] ——, "Self-similarity and long-range dependence in teletraffic," in *Proceedings of WSEAS International Conference. Mathematics and Computers in Science and Engineering*, no. 9. World Scientific and Engineering Academy and Society, 2009.

[46] J. Theiler, "Estimating fractal dimension," *JOSA A*, vol. 7, no. 6, pp. 1055–1073, 1990.

[47] T. Kalisky, Y. Ashkenazy, and S. Havlin, "Volatility of fractal and multifractal time series," *Israel Journal of Earth Sciences*, vol. 56, no. 1, pp. 47–56, 2007.

[48] R. Lopes and N. Betrouni, "Fractal and multifractal analysis: a review," *Medical Image Analysis*, vol. 13, no. 4, pp. 634–649, 2009.

[49] Y. Chen, M. Ding, and J. A. S. Kelso, "Long memory processes $1/f^{\alpha}$ type in human coordination," *Physical Review Letters*, vol. 79, no. 22, pp. 4501–4504, 1997.

[50] B. Pilgram and D. T. Kaplan, "A comparison of estimators for 1/f noise," *Physica D: Nonlinear Phenomena*, vol. 114, no. 1, pp. 108–122, 1998.

[51] M. J. Cannon, D. B. Percival, D. C. Caccia, G. M. Raymond, and J. B. Bassingthwaighte, "Evaluating scaled windowed variance methods for estimating the Hurst coefficient of time series," *Physica A: Statistical Mechanics and its Applications*, vol. 241, no. 3, pp. 606–626, 1997.

[52] R. B. Davies and D. Harte, "Tests for Hurst effect," *Biometrika*, vol. 74, no. 1, pp. 95–101, 1987.

[53] F. Crevecoeur, B. Bollens, C. Detrembleur, and T. Lejeune, "Towards a "gold-standard" approach to address the presence of long-range auto-correlation in physiological time series," *Journal of Neuroscience Methods*, vol. 192, no. 1, pp. 163–172, 2010.

[54] J. B. Bassingthwaighte and G. M. Raymond, "Evaluation of the dispersional analysis method for fractal time series," *Annals of Biomedical Engineering*, vol. 23, no. 4, pp. 491–505, 1995.

[55] ——, "Evaluating rescaled range analysis for time series," *Annals of Biomedical Engineering*, vol. 22, no. 4, pp. 432–444, 1994.

[56] ——, "Deriving dispersional and scaled windowed variance analyses using the correlation function of discrete fractional Gaussian noise," *Physica A: Statistical Mechanics and its Applications*, vol. 265, no. 1, pp. 85–96, 1999.

[57] C. K. Peng, S. V. Buldyrev, S. Havlin, M. Simons, H. E. Stanley, and A. L. Goldberger, "Mosaic organization of DNA nucleotides," *Physical Review E*, vol. 49, no. 2, p. 1685, 1994.

[58] J. M. Bardet and I. Kammoun, "Asymptotic properties of the detrended fluctuation analysis of long-range-dependent processes," *IEEE Transactions on Information Theory*, vol. 54, no. 5, pp. 2041–2052, 2008.

[59] D. C. Caccia, D. Percival, M. J. Cannon, G. Raymond, and J. B. Bassingthwaighte, "Analyzing exact fractal time series: evaluating dispersional analysis and rescaled range methods," *Physica A: Statistical Mechanics and its Applications*, vol. 246, no. 3, pp. 609–632, 1997.

[60] Z. Chen, P. C. Ivanov, K. Hu, and H. E. Stanley, "Effect of nonstationarities on detrended fluctuation analysis," *Physical Review E*, vol. 65, no. 4, p. 041107, 2002.

[61] C. Heneghan and G. McDarby, "Establishing the relation between detrended fluctuation analysis and power spectral density analysis for stochastic processes," *Physical Review E*, vol. 62, no. 5, p. 6103, 2000.

[62] K. Hu, P. C. Ivanov, Z. Chen, P. Carpena, and H. E. Stanley, "Effect of trends on detrended fluctuation analysis," *Physical Review E*, vol. 64, no. 1, p. 011114, 2001.

[63] J. W. Kantelhardt, E. Koscielny-Bunde, H. H. Rego, S. Havlin, and A. Bunde, "Detecting long-range correlations with detrended fluctuation analysis," *Physica A: Statistical Mechanics and its Applications*, vol. 295, no. 3, pp. 441–454, 2001.

[64] H. E. Schepers, J. H. Van Beek, and J. B. Bassingthwaighte, "Four methods to estimate the fractal dimension from self-affine signals (medical application)," *IEEE Engineering in Medicine and Biology Magazine*, vol. 11, no. 2, pp. 57–64, 1992.

[65] K. Willson and D. P. Francis, "A direct analytical demonstration of the essential equivalence of detrended fluctuation analysis and spectral analysis of RR interval variability," *Physiological Measurement*, vol. 24, no. 1, p. N1, 2003.

[66] P. F. Fougere, "On the accuracy of spectrum analysis of red noise processes using maximum entropy and periodogram methods: Simulation studies and application to geophysical data," *Journal of Geophysical Research*, vol. 90, no. A5, pp. 4355–4366, 1985.

[67] B. Audit, E. Bacry, J. F. Muzy, and A. Arneodo, "Wavelet-based estimators of scaling behavior," *IEEE Transactions on Information Theory*, vol. 48, no. 11, pp. 2938–2954, 2002.

[68] C. L. Jones, G. T. Lonergan, and D. E. Mainwaring, "Wavelet packet computation of the Hurst exponent," *Journal of Physics A: Mathematical and General*, vol. 29, no. 10, p. 2509, 1999.

[69] I. Simonsen, A. Hansen, and O. M. Nes, "Determination of the Hurst exponent by use of wavelet transforms," *Physical Review E*, vol. 58, no. 3, p. 2779, 1998.

[70] D. Veitch and P. Abry, "A wavelet-based joint estimator of the parameters of long-range dependence," *IEEE Transactions on Information Theory*, vol. 45, no. 3, pp. 878–897, 1999.

[71] A. Arneodo, Y. d'Aubenton Carafa, E. Bacry, P. Graves, J. Muzy, and C. Thermes, "Wavelet based fractal analysis of DNA sequences," *Physica D: Nonlinear Phenomena*, vol. 96, no. 1, pp. 291–320, 1996.

[72] S. G. Mallat, "A theory for multiresolution signal decomposition: the wavelet representation," *IEEE Transactions on Pattern Analysis and Machine Intelligence*, vol. 11, no. 7, pp. 674–693, 1989.